Effect of long-lived strongly interacting relic particles on big bang nucleosynthesis

Motohiko Kusakabe,[1,2,*,†] Toshitaka Kajino,[1,2,3] Takashi Yoshida,[2,‡] and Grant J. Mathews[4]

[1]*Department of Astronomy, Graduate School of Science, University of Tokyo, Bunkyo-ku, Tokyo 113-0033, Japan*
[2]*Division of Theoretical Astronomy, National Astronomical Observatory of Japan, Mitaka, Tokyo 181-8588, Japan*
[3]*Department of Astronomical Science, The Graduate University for Advanced Studies, Mitaka, Tokyo 181-8588, Japan*
[4]*Department of Physics, Center for Astrophysics, University of Notre Dame, Notre Dame, Indiana 46556, USA*

(Received 18 June 2009; published 2 November 2009)

It has been suggested that relic long-lived strongly interacting massive particles (SIMPs, or X particles) existed in the early universe. We study effects of such long-lived unstable SIMPs on big bang nucleosynthesis (BBN) assuming that such particles existed during the BBN epoch, but then decayed long before they could be detected. The interaction strength between an X particle and a nucleon is assumed to be similar to that between nucleons. We then calculate BBN in the presence of the unstable neutral charged X^0 particles taking into account the capture of X^0 particles by nuclei to form X nuclei. We also study the nuclear reactions and beta decays of X nuclei. We find that SIMPs form bound states with normal nuclei during a relatively early epoch of BBN. This leads to the production of heavy elements which remain attached to them. Constraints on the abundance of X^0 particles during BBN are derived from observationally inferred limits on the primordial light element abundances. Particle models which predict long-lived colored particles with lifetimes longer than ~200 s are rejected based upon these constraints.

DOI: 10.1103/PhysRevD.80.103501 PACS numbers: 26.35.+c, 95.35.+d, 98.80.Cq, 98.80.Es

I. INTRODUCTION

There has been considerable recent work on the effects of decay or annihilation of exotic particles on light element abundances [1–9]. Since standard big bang nucleosynthesis (BBN) predictions of light element abundances are more or less consistent with observations, changes of abundances relative to those of the standard BBN cannot be large. This makes it possible to constrain theories beyond the standard model through their consistency with observed light element abundances. Moreover, the decay process of massive particles might change the lithium abundances providing a solution to the lithium problems. Recent studies suggest that radiative decay could lead to the production of ^{6}Li to the level at most ~10 times larger than that observed in metal-poor halo stars (MPHSs) when the decay life is of the order of $\sim 10^8$–10^{12} s [9], and the hadronic decay can be a solution of both the lithium problems although that case gives a somewhat elevated deuterium abundance [3,8].

The possibility of the existence of heavy ($m \gg 1$ GeV) long-lived color flavored particles has been discussed in scenarios of split supersymmetry [10,11], and weak scale supersymmetry with a long-lived gluino [12] or squark [13] as the next-to-lightest supersymmetric particles. Those heavy partons would be confined at temperature below the deconfinement temperature $T_C \sim 180$ MeV inside exotic heavy hadrons, i.e., strongly interacting massive particles (SIMPs) [14]. Under the assumption that the X particles are in statistical equilibrium with the thermal background in the early universe, Kang *et al.* [14] estimated a relic abundance of those hadrons based upon a comparison between their annihilation rate and the Hubble expansion rate. In this way the estimated relic abundance can be written

$$\frac{N_X}{s} \sim 10^{-18}\left(\frac{R}{\mathrm{GeV}^{-1}}\right)^{-2}\left(\frac{T_B}{180\ \mathrm{MeV}}\right)^{-3/2}\left(\frac{m}{\mathrm{TeV}}\right)^{1/2}, \quad (1)$$

where N_X is the number density of the X particles, and $s = 2\pi^2 g_{*s} T^3/45$ is the entropy density with $g_{*s} \sim 10$ the total number of effective massless degrees of freedom [15] just below the QCD phase transition. T is the temperature of the expanding universe, R is the effective radius for annihilation of the X particles ($R \sim \mathrm{GeV}^{-1}$), T_B is the temperature at which the X particles are formed, and m is the mass ($m \gg 1$ GeV) of the heavy long-lived colored particles. This relic density corresponds to a number fraction of

$$Y_X \equiv N_X/n_b \sim 10^{-8}, \quad (2)$$

where n_b is the number density of baryons. We therefore assume the existence of the long-lived heavy hadronic particle X and study effects of such particles on BBN.

Experimental constraints on hypothetical SIMPs have been delineated in [16–18]. The effect of new neutral stable hadrons on BBN was studied in [19]. They assumed that the strong force between a nucleon and a stable hadron is similar to that between a nucleon and a Λ hyperon and that most new hadrons end up in a bound state of ^{4}He plus the hadron after BBN. The result of their analytical calculation showed that the stable hadrons would be preferentially

*kusakabe@icrr.u-tokyo.ac.jp
†Present address: Institute for Cosmic Ray Research, University of Tokyo, Kashiwa, Chiba 277-8582, Japan.
‡Present address: Department of Astronomy, Graduate School of Science, University of Tokyo, Bunkyo-ku, Tokyo 113-0033, Japan.

locked into beryllium. In other words, beryllium has the largest fraction A_X/A of bound states with the hadrons among the light elements produced in BBN, where the A and A_X represent a nuclide A and a bound state of A with a hadron X. Mohapatra and Teplitz [20] estimated the cross section for an X to be captured by ^{4}He and claimed that the fraction of hadronic X particles captured by ^{4}He nuclei is smaller than that assumed in [19]. Therefore a large fraction of free X particles would not become bound into light nuclides.

In this paper we carry out a consistent calculation of BBN in the presence of a hypothetical long-lived SIMP X^0 of charge zero assuming that the X^0 nucleon interaction is of a similar strength to that between two nucleons. Binding energies of bound states of X particles and nuclei, which we call X nuclei, are estimated. Rates for X capture by nuclides, as well as the nuclear reactions and β decay rates of X nuclei are also estimated. We calculate BBN including the X^0 particles as a new species taking account of many reactions related to X^0 particles in a network calculation, and study the effects of X^0 particles on BBN. In Sec. II assumptions regarding the X particle, estimations for binding energies of X nuclei, and various reaction rates are described. In Sec. III results of the network calculations are shown, and the constraints on parameters of the X^0 are derived from a comparison with observed primordial light element abundances. Conclusions of this work are summarized in Sec. IV.

II. MODEL

We have added the X particles and relevant X nuclei A_X as new species. Their reactions have been added to the BBN network code of Refs. [21,22]. Nuclear reaction rates for the standard BBN (SBBN) have been replaced with new rates published in Ref. [23] and the adopted neutron lifetime is $\tau_n = 881.9$ s [24]. Both proton and neutron captures and other nuclear reactions of X nuclei are taken into account. We have modified most of the thermonuclear reaction rates on the X nuclei from the original rates (without X nuclei). Binding energies between nuclei and X particles are of order $\sim$10 MeV. They are larger than those between a nucleus and massive particles which only interact electromagnetically of $\sim$0.1–1 MeV [25]. Hence, X particles lead to significant changes in reaction Q values for reactions involving X nuclei. Three possible effects of the binding of the X particles are: (1) changes in the Coulomb barriers resulting from the charge (if any) of the X particle in the nucleus; (2) modified reduced masses; and most importantly, (3) the modified Q values.

A. Properties of the X particle

The X^0 particle is assumed to be hadronic and to have zero electric charge and zero spin. Its mass is assumed to be much larger than the nucleon mass. We note that X^+ particles may also be present during BBN. Unlike the leptonic X^+ case, they could have a strong interaction with nuclei. However, there exists Coulomb repulsion leading to a certain degree of suppression of their reaction rates. Nevertheless, X^+ particles should eventually be included though we neglect them in the present investigation. Also, in this study, the nonthermal nucleosynthesis triggered by the later electromagnetic and/or hadronic decay is not studied. These effects will be addressed in a future publication. For now, however, as a first step we focus only on the effects of X^0 particles on BBN.

B. Nuclear binding energies

The nucleosynthesis of X nuclei is strongly dependent upon their binding energies. In our calculations, binding energies and eigenstate wave functions of X nuclei are computed taking into account the nuclear interaction and Coulomb interaction between the nucleus and the X particle. We assume that the potential is spherically symmetric. We then solve the two-body Schrödinger equation by a variational calculation (using the Gaussian expansion method [26]) to obtain binding energies.

The two-body Schrödinger equation for a spherically symmetric system is

$$\left(-\frac{\hbar^2}{2\mu}\nabla^2 + V(r) - E\right)\psi(r) = 0, \tag{3}$$

where $\hbar$ is Planck's constant, μ is the reduced mass, $V(r)$ is the central potential at r, E is the energy, and $\psi(r)$ is the wave function at r. Under the assumption that the X particle is much heavier than the light nuclides, μ is approximately given by the mass of the nuclide now considered. The central potential $V(r)$ is composed of a nuclear interaction $V_{\rm N}(r)$ and a Coulomb interaction $V_{\rm C}(r)$, i.e.,

$$V(r) = V_{\rm N}(r) + V_{\rm C}(r). \tag{4}$$

For the Coulomb potential, we assume that the charge distributions of the nuclei are Gaussian. We then use the charge radii determined from experiments of the corresponding nuclei (or neighboring nuclei when experimental data are not available). Here, we write

$$V_{\rm C}(r) = \frac{Z_A Z_X e^2}{r}\,{\rm erf}\left(\frac{r}{r_0}\right), \tag{5}$$

where $Z_A e$ and $Z_X e$ are the charges of nuclide A and X, respectively. The parameter r_0 is related to the mean square charge radius $\langle r_{\rm c}^2\rangle$ as $r_0 = \sqrt{2/3}\langle r_{\rm c}^2\rangle^{1/2}$, and ${\rm erf}(x) = (2/\sqrt{\pi})\int_0^x \exp(-t^2)dt$.

The X particle nucleon potential adopted here is assumed to be a square well of radius 2.5 fm and of depth of -25.5 MeV. This potential reproduces the binding energy of the deuteron i.e., 2.224 MeV. A Woods-Saxon potential is adopted for the nuclear potential between other nuclei and the X particles, i.e.,

$$V_{\rm N}(r) = -\frac{V_0}{1+\exp\{(r-R)/a\}}, \quad (6)$$

where the parameters are taken to be $V_0 = 50$ MeV, $a = 0.6$ fm and $R = \langle r_{\rm m}^2\rangle^{1/2}$. The mean square matter radii for nuclei, $\langle r_{\rm m}^2\rangle^{1/2}$, are taken from experiments of corresponding or neighboring nuclei. As a special case, the binding energy of two protons and an X particle system, i.e., pp_X, in a $1s$ orbit, is calculated with the same nuclear potential for the p_X and p system as that adopted for the estimation of the binding energy of ^{2}H and an X.

The adopted radii and obtained binding energies are listed in Table I. Binding energies in the case of neutral X^0, negatively charged X^- and positively charged X^+

TABLE I. Binding energies of X particles to nuclei.

Nuclide	$r_{\rm m}^{\rm RMS}$ (fm)[a]	Ref.	$r_{\rm c}^{\rm RMS}$ (fm)[b]	Ref.	$E_{\rm Bind}$ (MeV) X^0 case	X^- case	X^+ case
^1H_X	...	...	0.875 ± 0.007	[27]	9.242	10.103	8.391
^2H_X	1.971 ± 0.005	[28]	2.116 ± 0.006	[29]	24.570	25.344	23.798
^3H_X	1.657 ± 0.097[c]	[30]	1.755 ± 0.086	[30]	24.013	24.937	23.091
^2pp_X[d]	...	...	...	...	24.479	26.312	22.665
^3He_X	1.775 ± 0.034[c]	[30]	1.959 ± 0.030	[30]	25.819	27.526	24.117
^4He_X	1.59 ± 0.04	[31]	1.80 ± 0.04	[31]	25.621	27.491	23.756
^5He_X	2.52 ± 0.03[e]	[31]	2.38 ± 0.03[e]	[31]	38.221	39.697	36.748
^6He_X	2.52 ± 0.03	[31]	2.38 ± 0.03	[31]	39.235	40.724	37.748
^5Li_X	2.35 ± 0.03[f]	[31]	2.48 ± 0.03[f]	[31]	36.763	38.923	34.607
^6Li_X	2.35 ± 0.03	[31]	2.48 ± 0.03	[31]	37.853	40.031	35.679
^7Li_X	2.35 ± 0.03	[31]	2.43 ± 0.02	[31]	38.695	40.924	36.470
^8Li_X	2.38 ± 0.02	[31]	2.42 ± 0.02	[31]	39.610	41.856	37.368
^6Be_X	2.33 ± 0.02[g]	[31]	2.52 ± 0.02[g]	[31]	37.682	40.551	34.819
^7Be_X	2.33 ± 0.02	[31]	2.52 ± 0.02	[31]	38.528	41.415	35.647
^8Be_X	2.33 ± 0.02[g]	[31]	2.52 ± 0.02[g]	[31]	39.203	42.104	36.307
^9Be_X	2.38 ± 0.01	[31]	2.50 ± 0.01	[31]	40.153	43.080	37.231
$^{10}Be_X$	2.28 ± 0.02	[31]	2.40 ± 0.02	[31]	39.858	42.912	36.810
^7B_X	2.45 ± 0.10[h]	[32]	2.68 ± 0.12[h]	[32]	39.499	42.910	36.095
^8B_X	2.45 ± 0.10	[32]	2.68 ± 0.12	[32]	40.138	43.565	36.717
^9B_X	2.45 ± 0.10[h]	[32]	2.68 ± 0.12[h]	[32]	40.662	44.102	37.228
$^{10}B_X$	2.45 ± 0.10[h]	[32]	2.68 ± 0.12[h]	[32]	41.108	44.560	37.663
$^{11}B_X$	2.45 ± 0.10[h]	[32]	2.68 ± 0.12[h]	[32]	41.490	44.951	38.034
$^{12}B_X$	2.35 ± 0.02	[31]	2.51 ± 0.02	[31]	41.148	44.835	37.469
$^{10}C_X$	2.32 ± 0.02[i]	[31]	2.51 ± 0.02[i]	[31]	40.170	44.574	35.777
$^{11}C_X$	2.32 ± 0.02[i]	[31]	2.51 ± 0.02[i]	[31]	40.577	44.995	36.170
$^{12}C_X$	2.32 ± 0.02	[31]	2.51 ± 0.02	[31]	40.929	45.359	36.510
$^{13}C_X$	2.28 ± 0.04	[33]	2.463 ± 0.004	[34]	40.955	45.476	36.445
$^{14}C_X$	2.30 ± 0.07	[33]	2.496 ± 0.002	[34]	41.382	45.857	36.917
$^{12}N_X$	2.47 ± 0.07	[33]	2.62 ± 0.07[j]	[33]	41.952	46.906	37.012
$^{13}N_X$	2.31 ± 0.04	[33]	2.47 ± 0.04[j]	[33]	41.173	46.430	35.931
$^{14}N_X$	2.47 ± 0.03	[33]	2.56 ± 0.01	[34]	42.494	47.572	37.431
$^{15}N_X$	2.42 ± 0.10	[33]	2.61 ± 0.01	[34]	42.420	47.427	37.425
$^{14}O_X$	2.40 ± 0.03	[33]	2.56 ± 0.03[j]	[33]	42.058	47.886	36.247
$^{15}O_X$	2.44 ± 0.04	[33]	2.59 ± 0.04[j]	[33]	42.543	48.302	36.802
$^{16}O_X$	2.46 ± 0.12	[35]	2.71 ± 0.02	[35]	42.871	48.412	37.343

[a]Root mean square (RMS) nuclear matter radius.
[b]RMS charge radius.
[c]Derived by $(r_{\rm m}^{\rm RMS})^2 = (r_{\rm c}^{\rm RMS})^2 - (a_p^{\rm RMS})^2$ with $a_p^{\rm RMS} = 0.875 \pm 0.007$ fm using a RMS proton matter radius determined in experiment as a RMS charge radius.
[d]Estimated from the binding energies of ^1H_X plus Q values of the reaction $^1H_X(p,\gamma)pp_X$ (see text in Sec. II C 3).
[e]Taken from ^{6}He radius.
[f]Taken from ^{6}Li radius.
[g]Taken from ^{7}Be radius.
[h]Taken from ^{8}B radius.
[i]Taken from ^{12}C radius.
[j]Derived by $(r_{\rm c}^{\rm RMS})^2 = (r_{\rm m}^{\rm RMS})^2 + (a_p^{\rm RMS})^2$ with $a_p^{\rm RMS} = 0.875 \pm 0.007$ fm using a RMS matter radius determined in experiment.

particles are shown in columns 6, 7, and 8, respectively. The adopted root mean square (RMS) nuclear matter radii and their references are listed in columns 2 and 3. RMS charge radii and their references are shown in columns 4 and 5. Since the X particles are bound strongly to nuclei, their binding energies are typically large (~ 10 MeV), and are even larger for heavier nuclei. Hence, they are bound to nuclei from early in the BBN epoch. We note that their binding energies would be smaller (~ 0.1–1 MeV) if they could only bind electromagnetically to nuclei. In that case they would not be bound to nuclei until low temperature [$T_9 \equiv T/(10^9\ \mathrm{K}) \lesssim 0.3$]. The obtained binding energies are used for the estimation of Q values of various reactions as described below.

C. Reaction rates

1. Radiative X capture reactions

We assume that the rates of radiative neutral X^0 capture reactions by nuclei are roughly given by those of radiative neutron-capture reactions by the nuclides or neighboring nuclides (if there are no corresponding data). This assumption is introduced because we suppose that the X particles interact as strongly as normal nucleons. We correct the reduced mass and net charge for reactions involving X particles using the equations written below [Eqs. (7) and (8)]. The adopted reaction rates $N_A\langle\sigma v\rangle$, per second per mole cm^{-3}, are shown in Table II, where N_A is Avogadro's number. Reaction Q values are derived taking account of the binding energies of the X nuclei listed in Table I.

There are two noteworthy cases, $n(X,\gamma)n_X$ and $p(X,\gamma)p_X$. In the n plus neutral X^0 system, the electric multipole transitions do not occur because of charge neutrality. The magnetic dipole transition also disappears by the orthogonality condition between the scattering- and bound-s-wave states. Although only the magnetic quadrupole or higher multipole transitions are allowed, they are hindered by more than a factor of $\sim 10^6$ compared with allowed electric dipole transition for a photon energy of a few MeV. In the n plus charged $X^{\pm}$ system, the electric multipole transitions are allowed, but their transition probabilities disappear in the limit of a very massive X particle ($m \gg 1$ GeV). This is because the λ-multipole moment is proportional to $m^{-\lambda}$. The electric dipole transition rate, then, is very small for the reaction $n(X,\gamma)n_X$. Hence, we set the $n(X,\gamma)n_X$ rate to zero.

The nuclear potential for protons adopted in this study (Sec. II B) leads to only one bound $L = 0$ state with a binding energy of -9.2 MeV. Nuclei heavier than the nucleon can bind to the X particles in $L = 1$ excited states. In the system of p plus X, states exist with spin and parities of $J^\pi = 1/2^+$ (p) and 0^+ (X), thus leading to a bound state with $1/2^+$. There is then no possibility for an electric dipole transition, i.e., spin change $\Delta L = 1$ and a parity change from an s-wave relative orbital angular momentum between a p and an X. The electric dipole transition to the bound state from a p wave between the p and X is thus the dominant channel for the radiative capture reaction of a proton by an X particle. The rate of the $p(X,\gamma)p_X$ reaction has been estimated using the code RADCAP published by Bertulani [37] adopting the potential between a proton and an X particle as given in Sec. II B.

TABLE II. Rates of X^0 radiative capture reactions $A(X,\gamma)A_X$.

Product	Reaction rate (cm^3 s^{-1} mole^{-1})	Ref.	Reverse Coefficient[a]
^1n_X	0	⋯	0.987
$^1\mathrm{H}_X$	4×10^5	⋯[b]	0.987
$^2\mathrm{H}_X$	$7.4(1 + 18.9T_9)$	^{2}H	2.79
$^3\mathrm{H}_X$	4.2×10^2	^{6}Li	5.13
$^3\mathrm{He}_X$	$4.1 \times 10^{-1}(1 + 905T_9)$	^{3}He	5.13
$^4\mathrm{He}_X$	2.3×10^2	^{6}Li	7.89
$^6\mathrm{Li}_X$	1.0×10^2	^{6}Li	14.50
$^7\mathrm{Li}_X$	7.7×10^1	^{7}Li	18.27
$^8\mathrm{Li}_X$	5.9×10^1	^{7}Li	22.33
$^7\mathrm{Be}_X$	7.6×10^1	^{6}Li	18.27
$^9\mathrm{Be}_X$	1.0×10^1	^{9}Be[c]	26.64
$^8\mathrm{B}_X$	5.9×10^1	^{6}Li	22.33
$^{10}\mathrm{B}_X$	5.5×10^2	^{10}B	31.20
$^{11}\mathrm{B}_X$	5.1	^{11}B	36.00
$^{12}\mathrm{B}_X$	7.1×10^{-1}	^{13}C	41.02
$^{11}\mathrm{C}_X$	4.5×10^2	^{10}B	36.00
$^{12}\mathrm{C}_X$	2.7	^{12}C	41.02
$^{13}\mathrm{C}_X$	6.1×10^{-1}	^{13}C	46.25
$^{14}\mathrm{C}_X$	5.2×10^{-1}	^{13}C	51.69
$^{12}\mathrm{N}_X$	3.8×10^2	^{10}B	41.02
$^{13}\mathrm{N}_X$	2.3	^{12}C	46.25
$^{14}\mathrm{N}_X$	4.4×10^1	^{14}N	51.69
$^{15}\mathrm{N}_X$	1.3×10^{-2}	^{15}N[c]	57.32
$^{14}\mathrm{O}_X$	2.0	^{12}C	51.69
$^{15}\mathrm{O}_X$	3.8×10^1	^{14}N	57.32
$^{16}\mathrm{O}_X$	8.7×10^{-2}	^{16}O[c]	63.15

[a]For nucleus i with mass number A_i, the reverse coefficient is defined as in [36]. They are given by $0.9867A_i^{3/2}$ for the process $i(X,\gamma)i_X$ on the assumption that the X particle is much heavier than a nucleus.
[b]Approximate values calculated with a code RADCAP [37] at temperatures $T_9 \sim 2$–6.
[c]Taken from Ref. [38].

2. Nonresonant neutron-capture reactions of X nuclei

We include reactions between neutrons and X nuclei in the reaction network. We adopt known reaction rates for normal nuclei whenever possible. When the corresponding reaction rates are not available, rates of reactions for neighboring nuclei are adopted. For neutron-capture reactions at low energies, the s-wave interactions would dominate and the cross sections are proportional to the square of the de Broglie wavelength $\lambda\!\!\!^{-} = \hbar/(\mu v)$. We correct for the reduced mass and obtain neutron-induced reaction rates $\langle\sigma v\rangle_{A_X+n}$ given by

$$\langle\sigma v\rangle_{A_X+n} = \left(\frac{A_X}{A}\right)^{-2}\langle\sigma v\rangle_{A+n}, \tag{7}$$

where $\langle\sigma v\rangle_{A+n}$ is the neutron-capture reaction rate for the normal nucleus. A and A_X are the reduced masses for normal nuclei plus a neutron, and an X nucleus plus a neutron, respectively, in atomic mass units.

In the case of radiative neutron capture, i.e., $A_X(n,\gamma)B_X$, the electric dipole moment is very small similar to the $n(X,\gamma)n_X$ reaction. Hence, the higher electric quadrupole or magnetic dipole transitions contribute to the cross sections which are hindered by a factor of $\sim 10^3$ for emitted photon energies of order ~ 10 MeV. We adopt corresponding reaction rates for normal nuclei multiplied by 10^{-3} to account for this hindrance of radiative capture cross sections. Especially, the rate of the ${}^1\mathrm{H}_X(n,\gamma)^2\mathrm{H}_X$ reaction becomes negligibly small compared with that of the ${}^1\mathrm{H}_X(n,p)n_X$ reaction (see Table III), which predominantly processes ${}^1\mathrm{H}_X$.

3. Nonresonant reactions between charged particles

The leading term in the expression for thermonuclear reaction rates (TRR) $\langle\sigma v\rangle$ between charged particles can be roughly written (e.g., [39]) as

$$\langle\sigma v\rangle_{\mathrm{NR}} = \left(\frac{2}{AM_{\mathrm{u}}}\right)^{1/2} \frac{4E_0^{1/2}}{\sqrt{3}k_BT} S(E_0)\exp(-\tau), \qquad (8)$$

where $E_0 = 1.22(z_1^2Z_2^2AT_6^2)^{1/3}$ keV is the energy at the peak of the Gamow window, M_{u} is the atomic mass unit, $S(E_0)$ is the "astrophysical S factor" at E_0, k_B is the Boltzmann constant, T_6 is the temperature in units of 10^6 K, and

$$\tau = \frac{3E_0}{k_BT} = 42.46\left(\frac{z_1^2Z_2^2A}{T_6}\right)^{1/3}. \qquad (9)$$

The astrophysical S factor contains the nuclear matrix element for the reaction. We assume that the $S(E_0)$ values for reactions involving X nuclei are the same as those for the reactions of the corresponding normal nuclei [22,40,41]. When the corresponding S factors are not available, S factors of reactions for neighboring nuclei are adopted. Corrections for the TRR in the above equation arise from the reduced mass A. z_1 and Z_2 are the atomic numbers for the projectile normal nucleus and the target X

TABLE III. Radiative reaction rates for X^0 nuclei.

Reaction	Reaction rate ($\mathrm{cm^3\,s^{-1}\,mole^{-1}}$)	Reverse coefficient[a]	Q (MeV)
${}^1n_X(p,\gamma)^2\mathrm{H}_X$	4×10^5	1.32	17.553
${}^1\mathrm{H}_X(n,\gamma)^2\mathrm{H}_X$	1.2×10^1	1.32	17.553
${}^1\mathrm{H}_X(p,\gamma)^2pp_X$	$8\times10^7T_9^{-2/3}\exp(-4.25/T_9^{1/3})$[b]	3.95	15.237
${}^2\mathrm{H}_X(n,\gamma)^3\mathrm{H}_X$	$2.9\times10^{-2}(1+18.9T_9)$	2.96	5.700
${}^2\mathrm{H}_X(p,\gamma)^3\mathrm{He}_X$	$2.3\times10^3T_9^{-2/3}\exp(-4.25/T_9^{1/3})$	2.96	6.742
${}^3\mathrm{H}_X(p,\gamma)^4\mathrm{He}_X$	$2.0\times10^4T_9^{-2/3}\exp(-4.25/T_9^{1/3})$	3.95	21.422
${}^3\mathrm{He}_X(n,\gamma)^4\mathrm{He}_X$	$3.7\times10^{-3}(1+905.T_9)$	3.95	20.379
${}^3\mathrm{He}_X(\alpha,\gamma)^7\mathrm{Be}_X$	$3.6\times10^6T_9^{-2/3}\exp(-16.99/T_9^{1/3})$	3.95	17.346
${}^4\mathrm{He}_X(n,\gamma)^5\mathrm{He}_X$	3.7[c]	0.493	8.656
${}^4\mathrm{He}_X(p,\gamma)^5\mathrm{Li}_X$	$5.6\times10^5T_9^{-2/3}\exp(-6.74/T_9^{1/3})$[d]	0.493	9.176
${}^4\mathrm{He}_X(d,\gamma)^6\mathrm{Li}_X$	$2.6\times10^1T_9^{-2/3}\exp(-8.50/T_9^{1/3})$	2.79	13.706
${}^4\mathrm{He}_X(t,\gamma)^7\mathrm{Li}_X$	$2.5\times10^5T_9^{-2/3}\exp(-9.73/T_9^{1/3})$	2.56	15.541
${}^4\mathrm{He}_X({}^3\mathrm{He},\gamma)^7\mathrm{Be}_X$	$4.0\times10^6T_9^{-2/3}\exp(-15.44/T_9^{1/3})$	2.56	14.494
${}^4\mathrm{He}_X(\alpha,\gamma)^8\mathrm{Be}_X$	$3.6\times10^6T_9^{-2/3}\exp(-16.99/T_9^{1/3})$[e]	7.89	13.490
${}^4\mathrm{He}_X({}^6\mathrm{Li},\gamma)^{10}\mathrm{B}_X$	$3.0\times10^6T_9^{-2/3}\exp(-25.49/T_9^{1/3})$	6.22	19.949
${}^5\mathrm{He}_X(n,\gamma)^6\mathrm{He}_X$	3.7[c]	7.89	2.880
${}^5\mathrm{He}_X(p,\gamma)^6\mathrm{Li}_X$	$5.6\times10^5T_9^{-2/3}\exp(-6.74/T_9^{1/3})$[d]	2.63	4.224
${}^6\mathrm{He}_X(p,\gamma)^7\mathrm{Li}_X$	$5.6\times10^5T_9^{-2/3}\exp(-6.74/T_9^{1/3})$[d]	0.493	9.436
${}^5\mathrm{Li}_X(n,\gamma)^6\mathrm{Li}_X$	3.7[c]	2.63	6.754
${}^5\mathrm{Li}_X(p,\gamma)^6\mathrm{Be}_X$	$6.4\times10^5T_9^{-2/3}\exp(-8.84/T_9^{1/3})$[d]	7.89	1.513
${}^6\mathrm{Li}_X(n,\gamma)^7\mathrm{Li}_X$	3.7	1.48	8.092
${}^6\mathrm{Li}_X(p,\gamma)^7\mathrm{Be}_X$	$6.4\times10^5T_9^{-2/3}\exp(-8.84/T_9^{1/3})$	1.48	6.281
${}^6\mathrm{Li}_X(\alpha,\gamma)^{10}\mathrm{B}_X$	$3.4\times10^6T_9^{-2/3}\exp(-22.27/T_9^{1/3})$	3.38	7.716
${}^7\mathrm{Li}_X(n,\gamma)^8\mathrm{Li}_X$	3.8	1.58	2.947
${}^7\mathrm{Li}_X(p,\gamma)^8\mathrm{Be}_X$	$1.7\times10^7T_9^{-2/3}\exp(-8.84/T_9^{1/3})$	7.89	17.763
${}^7\mathrm{Li}_X(\alpha,\gamma)^{11}\mathrm{B}_X$	$3.1\times10^7T_9^{-2/3}\exp(-22.27/T_9^{1/3})$	7.89	11.460
${}^8\mathrm{Li}_X(p,\gamma)^9\mathrm{Be}_X$	$1.7\times10^7T_9^{-2/3}\exp(-8.84/T_9^{1/3})$[f]	2.47	17.431
${}^6\mathrm{Be}_X(n,\gamma)^7\mathrm{Be}_X$	3.7[c]	0.493	11.522
${}^7\mathrm{Be}_X(n,\gamma)^8\mathrm{Be}_X$	3.7[c]	7.89	19.574
${}^7\mathrm{Be}_X(p,\gamma)^8\mathrm{B}_X$	$3.0\times10^5T_9^{-2/3}\exp(-10.71/T_9^{1/3})$	1.58	1.747
${}^7\mathrm{Be}_X(\alpha,\gamma)^{11}\mathrm{C}_X$	$7.3\times10^7T_9^{-2/3}\exp(-25.87/T_9^{1/3})$	7.89	9.539

TABLE III. (*Continued*)

Reaction	Reaction rate ($cm^3\ s^{-1}\ mole^{-1}$)	Reverse coefficient[a]	Q (MeV)
$^8Be_X(n,\gamma)^9Be_X$	3.8[g]	0.493	2.615
$^8Be_X(p,\gamma)^9B_X$	$3.0\times10^5 T_9^{-2/3}\exp(-10.71/T_9^{1/3})$[h]	0.493	1.274
$^9Be_X(n,\gamma)^{10}Be_X$	8.2×10^{-1}[i]	7.89	6.518
$^9Be_X(p,\gamma)^{10}B_X$	$1.3\times10^7 T_9^{-2/3}\exp(-10.71/T_9^{1/3})$	1.13	7.542
$^{10}Be_X(p,\gamma)^{11}B_X$	$1.3\times10^7 T_9^{-2/3}\exp(-10.71/T_9^{1/3})$[j]	0.493	12.859
$^8B_X(n,\gamma)^9B_X$	3.7[k]	2.47	19.101
$^9B_X(n,\gamma)^{10}B_X$	3.8[g]	1.13	8.883
$^9B_X(p,\gamma)^{10}C_X$	$4.5\times10^5 T_9^{-2/3}\exp(-12.42/T_9^{1/3})$[l]	7.89	3.514
$^{10}B_X(n,\gamma)^{11}B_X$	5.5×10^1	3.45	11.835
$^{10}B_X(p,\gamma)^{11}C_X$	$4.5\times10^5 T_9^{-2/3}\exp(-12.42/T_9^{1/3})$	3.45	8.158
$^{11}B_X(n,\gamma)^{12}B_X$	6.1×10^{-1}	2.63	3.029
$^{11}B_X(p,\gamma)^{12}C_X$	$4.5\times10^7 T_9^{-2/3}\exp(-12.42/T_9^{1/3})$	7.89	15.396
$^{10}C_X(n,\gamma)^{11}C_X$	3.8[m]	0.493	13.527
$^{11}C_X(n,\gamma)^{12}C_X$	5.5×10^1[n]	7.89	19.074
$^{11}C_X(p,\gamma)^{12}N_X$	$4.1\times10^4 T_9^{-2/3}\exp(-14.03/T_9^{1/3})$	2.63	1.977
$^{12}C_X(n,\gamma)^{13}C_X$	3.8×10^{-1}	0.987	4.972
$^{12}C_X(p,\gamma)^{13}N_X$	$2.0\times10^7 T_9^{-2/3}\exp(-14.03/T_9^{1/3})$	0.987	2.187
$^{12}C_X(\alpha,\gamma)^{16}O_X$	$9.4\times10^7 T_9^{-2/3}\exp(-35.35/T_9^{1/3})$	7.89	9.104
$^{13}C_X(n,\gamma)^{14}C_X$	1.0×10^{-1}	3.95	8.603
$^{13}C_X(p,\gamma)^{14}N_X$	$7.8\times10^7 T_9^{-2/3}\exp(-14.03/T_9^{1/3})$	1.32	9.089
$^{14}C_X(p,\gamma)^{15}N_X$	$6.6\times10^6 T_9^{-2/3}\exp(-14.03/T_9^{1/3})$	0.987	11.245
$^{13}N_X(p,\gamma)^{14}O_X$	$3.9\times10^7 T_9^{-2/3}\exp(-15.55/T_9^{1/3})$	3.95	5.512
$^{14}N_X(n,\gamma)^{15}N_X$	8.7	2.96	10.759
$^{14}N_X(p,\gamma)^{15}O_X$	$4.8\times10^7 T_9^{-2/3}\exp(-15.55/T_9^{1/3})$	2.96	7.346
$^{15}N_X(p,\gamma)^{16}O_X$	$9.6\times10^8 T_9^{-2/3}\exp(-15.55/T_9^{1/3})$	3.95	12.578

[a]For nuclides $a = i, j, k, \ldots$ with mass numbers A_a and numbers of magnetic substates g_a, the reverse coefficients are defined as in [36]: on the assumption that an X particle is much heavier than nuclides, they are given by $0.9867(g_i g_j/g_k)A_j^{3/2}$ for the process $i_X(j,\gamma)k_X$.
[b]The approximate values calculated with a code RADCAP [37] at temperatures $T_9 \sim 2$–6.
[c]The rate of the reaction $^6Li(n,\gamma)^7Li$ multiplied by 10^{-3} is used.
[d]The S factor for the reaction $^6Li(p,\gamma)^7Be$ is used.
[e]The S factor for the reaction $^3He(\alpha,\gamma)^7Be$ is used.
[f]The S factor for the reaction $^7Li(p,\gamma)^8Be$ is used.
[g]The rate of the reaction $^7Li(n,\gamma)^8Li$ multiplied by 10^{-3} is used.
[h]The S factor for the reaction $^7Be(p,\gamma)^8B$ is used.
[i]The cross section from [38] multiplied by 10^{-3} is used.
[j]The S factor for the reaction $^9Be(p,\gamma)^{10}B$ is used.
[k]The cross section from [38] multiplied by 10^{-3} is used.
[l]The S factor for the reaction $^{10}B(p,\gamma)^{11}C$ is used.
[m]The rate of the reaction $^7Li(n,\gamma)^8Li$ multiplied by 10^{-3} is used.
[n]The rate of the reaction $^{10}B(n,\gamma)^{11}B$ multiplied by 10^{-3} is used.

nucleus, respectively. Note that we have taken the spin of the X particles to be zero in this study.

Rates for two reactions, $p_X(p,\gamma)pp_X$ and $n_X(p,\gamma)^2H_X$, are calculated with the code RADCAP [37]. The adopted nuclear potential is that of the d plus X system (Sec. II B) for both reactions.

The adopted reaction rates $N_A\langle\sigma v\rangle_{\rm NR}$, thus obtained, are shown in Table III for radiative reactions, Table IV is for nonradiative reactions independent of the deuteron, and Table V is for deuteron capture nonradiative reactions.

4. Rates for reactions with negative Q values

We find that there are several reactions whose Q values become negative when nuclei are bound to X particles. We neglect most of those reactions except for the $^3H_X(p,n)^3He_X$, $^4He_X(t,n)^6Li_X$, and $^4He_X(^3He,p)^6Li_X$ reactions. However, neglected reactions might be important and should eventually be included in our calculation. The rates of these three reactions are given by the Hauser-Feshbach approximation as follows. For a compound-nucleus reaction

$$1 + 2 \rightarrow C \rightarrow 3 + 4 + Q, \tag{10}$$

where C is the compound nucleus, the cross section is given by the product of the probability of formation of the compound nucleus from $1 + 2$, and that of its decay into the $3 + 4$ particle channel, i.e.

TABLE IV. Nonradiative reaction rates for X^0 nuclei.

Reaction	Reaction rate ($cm^3\ s^{-1}\ mole^{-1}$)	Reverse coefficient[a]	Q (MeV)
$^1H_X(n, p)^1n_X$	2.0×10^{9}[b]	1.0	0.0
$^2pp_X(n, p)^2H_X$	2.0×10^{9}[b]	0.333	2.316
$^1H_X(\alpha, p)^4He_X$	$2.8 \times 10^{11} T_9^{-2/3} \exp(-10.71/T_9^{1/3})$[c]	8.0	11.150
$^3H_X(p, n)^3He_X$	$2.5 \times 10^{10} T_9^{-2/3} \exp(-4.25/T_9^{1/3})$	1.0	1.043
$^4He_X(t, n)^6Li_X$	$8.7 \times 10^{10} T_9^{-2/3} \exp(-9.73/T_9^{1/3})$	1.73	7.449
$^4He_X(^3He_X, p)^6Li_X$	$1.1 \times 10^{11} T_9^{-2/3} \exp(-15.44/T_9^{1/3})$	1.73	8.213
$^5Li_X(n, p)^5He_X$	2.0×10^{9}[b]	1.0	2.530
$^7Li_X(p, \alpha)^4He_X$	$1.0 \times 10^{9} T_9^{-2/3} \exp(-8.84/T_9^{1/3})$	1.00	4.273
$^8Li_X(p, n)^8Be_X$	$8.3 \times 10^{9} T_9^{-2/3} \exp(-11.13/T_9^{1/3})$[d]	5.0	14.816
$^8Li_X(p, \alpha)^5He_X$	$1.0 \times 10^{9} T_9^{-2/3} \exp(-11.13/T_9^{1/3})$[e]	0.313	13.032
$^8Li_X(\alpha, n)^{11}B_X$	$7.5 \times 10^{13} T_9^{-2/3} \exp(-22.27/T_9^{1/3})$	5.0	8.512
$^6Be_X(n, p)^6Li_X$	2.0×10^{9}[b]	0.333	5.241
$^7Be_X(n, p)^7Li_X$	2.0×10^{9}	1.00	1.810
$^6Be_X(\alpha, n)^{12}C_X$	$4.1 \times 10^{13} T_9^{-2/3} \exp(-26.98/T_9^{1/3})$	16.00	6.477
$^8B_X(n, p)^8Be_X$	3.2×10^{8}[f]	5.0	17.827
$^8B_X(\alpha, p)^{11}C_X$	$9.4 \times 10^{14} T_9^{-2/3} \exp(-31.30/T_9^{1/3})$	5.00	7.846
$^9B_X(n, p)^9Be_X$	2.0×10^{9}[b]	1.0	1.341
$^9B_X(n, \alpha)^6Li_X$	4.2×10^{8}[g]	0.333	13.539
$^{10}B_X(\alpha, n^{13}N_X)$	$1.1 \times 10^{13} T_9^{-2/3} \exp(-31.30/T_9^{1/3})$	14.0	1.123
$^{10}B_X(\alpha, p)^{13}C_X$	$8.6 \times 10^{14} T_9^{-2/3} \exp(-31.30/T_9^{1/3})$	14.0	3.908
$^{11}B_X(p, \alpha)^8Be_X$	$2.0 \times 10^{11} T_9^{-2/3} \exp(-12.42/T_9^{1/3})$[h]	1.0	6.303
$^{11}B_X(\alpha, n)^{14}N_X$	$6.3 \times 10^{12} T_9^{-2/3} \exp(-31.30/T_9^{1/3})$	5.33	1.162
$^{11}B_X(\alpha, p)^{14}C_X$	$4.8 \times 10^{11} T_9^{-2/3} \exp(-31.30/T_9^{1/3})$	16.0	0.676
$^{12}B_X(p, n)^{12}C_X$	$3.9 \times 10^{11} T_9^{-2/3} \exp(-12.42/T_9^{1/3})$	3.00	12.367
$^{12}B_X(p, \alpha)^9Be_X$	$2.0 \times 10^{11} T_9^{-2/3} \exp(-12.42/T_9^{1/3})$	0.188	5.889
$^{12}B_X(\alpha, n)^{15}N_X$	$2.8 \times 10^{15} T_9^{-2/3} \exp(-31.30/T_9^{1/3})$	6.00	8.892
$^{10}C_X(n, p)^{10}B_X$	2.0×10^{9}[b]	0.143	5.369
$^{10}C_X(n, \alpha)^7Be_X$	4.2×10^{8}[g]	0.0625	3.933
$^{11}C_X(n, p)^{11}B_X$	1.4×10^{8}	1.0	3.677
$^{11}C_X(n, \alpha)^8Be_X$	1.3×10^{8}[i]	1.0	9.981
$^{11}C_X(\alpha, p)^{14}N_X$	$6.4 \times 10^{15} T_9^{-2/3} \exp(-35.35/T_9^{1/3})$	5.33	4.840
$^{13}C_X(\alpha, n)^{16}O_X$	$6.2 \times 10^{15} T_9^{-2/3} \exp(-35.35/T_9^{1/3})$	8.00	4.131
$^{12}N_X(n, p)^{12}C_X$	1.4×10^{8}[j]	3.0	17.097
$^{12}N_X(n, \alpha)^9B_X$	4.2×10^{8}[k]	0.188	9.278
$^{12}N_X(\alpha, p)^{15}O_X$	$5.1 \times 10^{16} T_9^{-2/3} \exp(-39.18/T_9^{1/3})$	6.00	10.209
$^{13}N_X(n, p)^{13}C_X$	1.6×10^{8}	1.00	2.049
$^{13}N_X(\alpha, p)^{16}O_X$	$3.0 \times 10^{17} T_9^{-2/3} \exp(-39.18/T_9^{1/3})$	8.00	6.916
$^{15}N_X(p, \alpha)^{12}C_X$	$1.1 \times 10^{12} T_9^{-2/3} \exp(-15.55/T_9^{1/3})$	0.500	3.474
$^{15}O_X(n, p)^{15}N_X$	3.1×10^{8}	1.00	3.413
$^{15}O_X(n, \alpha)^{12}C_X$	3.1×10^{7}	0.500	6.888

[a]For nuclides $a = i, j, k, \ldots$ with mass numbers A_a and numbers of magnetic substates g_a, the reverse coefficients are defined as in [36]: on the assumption that an X particle is much heavier than nuclides, they are given by $(g_i g_j/(g_k g_l))(A_j/A_k)^{3/2}$ for the process $i_X(j, k)l_X$.
[b]The rate of the reaction $^7Be(n, p)^7Li$ is used.
[c]The S factor for the reaction $^8B(d, p)^{11}C$ is used.
[d]The S factor for the reaction $^8Li(p, n\alpha)^4He$ is used.
[e]The S factor for the reaction $^7Li(p, \alpha)^4He$ is used.
[f]The rate of the reaction $^8B(n, p\alpha)^4He$ is used.
[g]The rate of the reaction $^{10}Be(n, \alpha)^7Li$ is used.
[h]The S factor for the reaction $^{12}B(p, \alpha)^9Be$ is used.
[i]The rate of the reaction $^{11}C(n, 2\alpha)^4He$ is used.
[j]The rate of the reaction $^{11}C(n, p)^{11}B$ is used.
[k]The rate of the reaction $^{10}B(n, \alpha)^7Li$ is used.

TABLE V. (d, n) and (d, p) reaction rates for X^0 nuclei.

Reaction	Reaction rate ($\mathrm{cm^3\ s^{-1}\ mole^{-1}}$)	Reverse coefficient[a]	Q (MeV)
$^2H_X(d, n)^3H_X$	$3.3 \times 10^8 T_9^{-2/3} \exp(-5.35/T_9^{1/3})$	6.364	2.182
$^2H_X(d, p)^3He_X$	$3.1 \times 10^8 T_9^{-2/3} \exp(-5.35/T_9^{1/3})$	6.364	5.811
$^3H_X(d, n)^4He_X$	$9.0 \times 10^{10} T_9^{-2/3} \exp(-5.35/T_9^{1/3})$	8.485	19.197
$^3He_X(d, p)^4He_X$	$4.2 \times 10^{10} T_9^{-2/3} \exp(-8.50/T_9^{1/3})$	8.49	18.154
$^4He_X(d, n)^5Li_X$	$1.1 \times 10^{11} T_9^{-2/3} \exp(-8.50/T_9^{1/3})$[b]	1.061	6.952
$^4He_X(d, p)^5He_X$	$4.2 \times 10^{10} T_9^{-2/3} \exp(-8.50/T_9^{1/3})$[c]	1.061	9.482
$^5He_X(d, n)^6Li_X$	$1.1 \times 10^{11} T_9^{-2/3} \exp(-8.50/T_9^{1/3})$[b]	5.657	2.000
$^5He_X(d, p)^6He_X$	$4.2 \times 10^{10} T_9^{-2/3} \exp(-8.50/T_9^{1/3})$[c]	16.97	0.655
$^6He_X(d, n)^7Li_X$	$2.3 \times 10^{11} T_9^{-2/3} \exp(-8.50/T_9^{1/3})$[d]	1.061	7.211
$^5Li_X(d, p)^6Li_X$	$4.8 \times 10^{10} T_9^{-2/3} \exp(-11.13/T_9^{1/3})$[c]	5.657	4.530
$^6Li_X(d, n)^7Be_X$	$2.7 \times 10^{11} T_9^{-2/3} \exp(-11.13/T_9^{1/3})$[d]	3.182	4.056
$^6Li_X(d, p)^7Li_X$	$8.9 \times 10^{11} T_9^{-2/3} \exp(-11.13/T_9^{1/3})$[e]	3.182	5.867
$^7Li_X(d, n)^8Be_X$	$2.7 \times 10^{11} T_9^{-2/3} \exp(-11.13/T_9^{1/3})$[d]	16.97	15.539
$^7Li_X(d, p)^8Li_X$	$8.9 \times 10^{11} T_9^{-2/3} \exp(-11.13/T_9^{1/3})$[e]	3.394	0.723
$^8Li_X(d, n)^9Be_X$	$2.7 \times 10^{11} T_9^{-2/3} \exp(-11.13/T_9^{1/3})$[d]	5.303	15.206
$^6Be_X(d, p)^7Be_X$	$9.8 \times 10^{11} T_9^{-2/3} \exp(-13.49/T_9^{1/3})$[e]	1.061	9.298
$^7Be_X(d, p)^8Be_X$	$9.8 \times 10^{11} T_9^{-2/3} \exp(-13.49/T_9^{1/3})$[e]	16.97	17.350
$^8Be_X(d, p)^9Be_X$	$9.8 \times 10^{11} T_9^{-2/3} \exp(-13.49/T_9^{1/3})$[e]	1.060	0.391
$^9Be_X(d, n)^{10}B_X$	$4.2 \times 10^{11} T_9^{-2/3} \exp(-13.49/T_9^{1/3})$	2.424	5.317
$^8B_X(d, p)^9B_X$	$1.1 \times 10^{11} T_9^{-2/3} \exp(-15.65/T_9^{1/3})$ [e]	5.303	16.877
$^9B_X(d, n)^{10}C_X$	$4.5 \times 10^{11} T_9^{-2/3} \exp(-15.65/T_9^{1/3})$[f]	16.97	1.290
$^9B_X(d, p)^{10}B_X$	$1.3 \times 10^{12} T_9^{-2/3} \exp(-15.65/T_9^{1/3})$[g]	2.424	6.658
$^{10}B_X(d, n)^{11}C_X$	$2.2 \times 10^{12} T_9^{-2/3} \exp(-15.65/T_9^{1/3})$[h]	7.425	5.933
$^{10}B_X(d, p)^{11}B_X$	$1.3 \times 10^{12} T_9^{-2/3} \exp(-15.65/T_9^{1/3})$	7.425	9.611
$^{11}B_X(d, n)^{12}C_X$	$2.2 \times 10^{12} T_9^{-2/3} \exp(-15.65/T_9^{1/3})$[h]	16.97	13.172
$^{11}B_X(d, p)^{12}B_X$	$1.3 \times 10^{12} T_9^{-2/3} \exp(-15.65/T_9^{1/3})$[g]	5.657	0.805
$^{12}B_X(d, n)^{13}C_X$	$2.2 \times 10^{12} T_9^{-2/3} \exp(-15.65/T_9^{1/3})$[h]	6.364	15.115
$^{10}C_X(d, p)^{11}C_X$	$1.4 \times 10^{12} T_9^{-2/3} \exp(-17.67/T_9^{1/3})$[g]	1.061	11.302
$^{11}C_X(d, p)^{12}C_X$	$1.4 \times 10^{12} T_9^{-2/3} \exp(-17.67/T_9^{1/3})$[g]	16.97	16.849
$^{12}C_X(d, p)^{13}C_X$	$1.4 \times 10^{12} T_9^{-2/3} \exp(-17.67/T_9^{1/3})$[g]	2.121	2.748
$^{13}C_X(d, n)^{14}N_X$	$2.3 \times 10^{12} T_9^{-2/3} \exp(-17.67/T_9^{1/3})$[h]	2.828	6.865
$^{13}C_X(d, p)^{14}C_X$	$1.4 \times 10^{12} T_9^{-2/3} \exp(-17.67/T_9^{1/3})$[g]	8.485	6.379
$^{14}C_X(d, n)^{15}N_X$	$2.3 \times 10^{12} T_9^{-2/3} \exp(-17.67/T_9^{1/3})$[h]	2.121	9.021
$^{12}N_X(d, p)^{13}N_X$	$1.5 \times 10^{12} T_9^{-2/3} \exp(-19.59/T_9^{1/3})$[g]	6.364	17.060
$^{13}N_X(d, n)^{14}O_X$	$2.4 \times 10^{12} T_9^{-2/3} \exp(-19.59/T_9^{1/3})$[h]	8.485	3.288
$^{13}N_X(d, p)^{14}N_X$	$1.5 \times 10^{12} T_9^{-2/3} \exp(-19.59/T_9^{1/3})$[g]	2.828	9.650
$^{14}N_X(d, n)^{15}O_X$	$2.4 \times 10^{12} T_9^{-2/3} \exp(-19.59/T_9^{1/3})$[h]	6.364	5.122
$^{14}N_X(d, p)^{15}N_X$	$1.5 \times 10^{12} T_9^{-2/3} \exp(-19.59/T_9^{1/3})$[g]	6.364	8.535
$^{15}N_X(d, n)^{16}O_X$	$2.4 \times 10^{12} T_9^{-2/3} \exp(-19.59/T_9^{1/3})$[h]	8.485	10.354

[a]For nuclides $a = i, j, k, \ldots$ with mass numbers A_a and numbers of magnetic substates g_a, the reverse coefficients are defined as in [36]: on the assumption that an X particle is much heavier than nuclides, they are given by $(g_i g_j/(g_k g_l))(A_j/A_k)^{3/2}$ for the process $i_X(j, k)l_X$.
[b]The S factor for the reaction $^3H(d, n)^4He$ is used.
[c]The S factor for the reaction $^3He(d, p)^4He$ is used.
[d]The S factor for the reaction $^7Li(d, n\alpha)^4He$ is used.
[e]The S factor for the reaction $^7Be(d, p\alpha)^4He$ is used.
[f]The S factor for the reaction $^9Be(d, n)^{10}B$ is used.
[g]The S factor for the reaction $^{10}Be(d, p)^{11}B$ is used.
[h]The S factor for the reaction $^{11}B(d, n)^{12}C$ is used.

$$\sigma = (1 + \delta_{12})\pi\lambda\!\!\!^{-2}_{12} \frac{1}{(2I_1 + 1)(2I_2 + 1)} \times \sum_{I_1, I_2, I_3, I_4} |\langle 3, 4|H_{\mathrm{II}}|C\rangle\langle C|H_{\mathrm{I}}|1, 2\rangle|^2, \quad (11)$$

where I_i is the spin of the nucleus i, and $\lambda\!\!\!^{-}_{12}$ is the de Broglie wavelength of the entrance channel [e.g., Eq. (3.9.26) in Ref. [39]] satisfying

$$\pi\lambda\!\!\!^{-2}_{ij} = \frac{657}{A_{ij}E_{ij,\mathrm{keV}}}\ \mathrm{barn}. \quad (12)$$

The factor $(1 + \delta_{ij})$ doubles the cross section for indistin-

guishable particles. The matrix elements in angle brackets have information on the nuclear factors (and the Coulomb barrier penetration probabilities if they are reactions between charged particles). The barrier penetration probability for s waves in the low-energy limit is given [e.g., Eq. (3.10.10) in Ref. [39]] by

$$P_{ij} \approx \left(\frac{E_C}{E_{ij}}\right)^{1/2} \exp\left(-\frac{2\pi z_i Z_j e^2}{\hbar v_{ij}} + 4\left(\frac{E_C}{\hbar^2/2\mu R_{ij}^2}\right)^{1/2}\right)$$
$$= \left(\frac{E_C}{E_{ij}}\right)^{1/2} \exp\left(-31.28\frac{z_i Z_j A_{ij,X}^{1/2}}{E_{ij,\mathrm{keV}}^{1/2}} + 1.05(A_{ij,X} R_{ij,\mathrm{fm}} z_i Z_j)^{1/2}\right), \quad (13)$$

where $z_i e$ and $Z_j e$ are the charges of nuclei i and j_X, respectively, $A_{ij,X}$ is the reduced mass, E_{ij} and $E_{ij,\mathrm{keV}}$ denotes the center of mass energy, where units of keV are indicated where used. v_{ij} is the relative velocity of the projectile target system of i and j_X. $R_{ij} = 1.4(A_i^{1/3} + A_j^{1/3})$ fm is the contact nuclear radius, i.e. the separation between the centers of particle i and j_X when the attractive nuclear force overcomes the Coulomb barrier. Here A_i and A_j are the masses of nuclides i and j in atomic mass units. $R_{ij,\mathrm{fm}}$ is the R_{ij} value in units of fm. $E_C = 1.44 z_i Z_j / R_{ij,\mathrm{fm}}$ MeV is the height of the Coulomb barrier. The penetration probabilities are contained in the matrix elements. Defining partial widths Γ_a and Γ_b of the compound nucleus for decays into entrance and exit channels, respectively, the cross section for the reaction Eq. (10) has a scaling relation of

$$\sigma_{ij} \propto \lambda_{ij}^2 \Gamma_a \Gamma_b \propto \frac{\Gamma_a \Gamma_b}{A_{ij} E_{ij}}. \quad (14)$$

The partial width for the particle decay channel can be written [42] as

$$\Gamma = \frac{3\hbar v}{R} P \theta^2, \quad (15)$$

where θ^2 is the dimensionless reduced width, i.e., a measure of the degree to which the compound nuclear state can be described by the relative motion of i and j in a potential. For reactions of X nuclei, we assume that the nuclear radius R and the reduced width θ^2 are the same as those for the corresponding normal reactions. The cross section, therefore, scales according to

$$\sigma_{12} \propto \frac{(v_{12} P_{12})(v_{34} P_{34})}{A_{12} E_{12}}. \quad (16)$$

We use this scaling relation and adopt coefficients in Eq. (16) from the standard nuclear reactions assuming that the coefficients contain the information of the purely nuclear part and that other parts including Coulomb penetration factors related to corrected reaction Q values can be extracted as in Eq. (16).

The dimensionless reduced width θ^2 is also related to the spectroscopic factor for a direct reaction [39]. The distinction between a compound nucleus and a direct reaction can be obscure as low-energy direct reactions can result from many overlapping resonances.

For the reaction ${}^3\mathrm{H}_X(p, n){}^3\mathrm{He}_X$, we adopt the nonresonant rate of the normal reaction ${}^3\mathrm{He}(n, p){}^3\mathrm{H}$, i.e., $N_A\langle\sigma v\rangle_{\mathrm{SBBN}} = 7.21 \times 10^8\ \mathrm{cm^3\ s^{-1}\ mole^{-1}}$ [21]. The penetration factor for the exit channel for ${}^3\mathrm{He}(n, p){}^3\mathrm{H}$ is assumed to be $P_p = 1$ because of the high Q value ($Q > E_C$). Equation (16) leads to the following S factor for the ${}^3\mathrm{H}_X(p, n){}^3\mathrm{He}_X$ reaction:

$$S_{{}^3\mathrm{H}_X + p} \equiv \frac{\sigma E}{\exp(-2\pi\eta)} = 3.1\ \mathrm{MeV\,barn}, \quad (17)$$

where $\eta \equiv z_1 Z_2 e^2/(\hbar v)$.

For the reaction ${}^4\mathrm{He}_X(t, n){}^6\mathrm{Li}_X$, we adopt the nonresonant rate of the ${}^6\mathrm{Li}(n, \alpha){}^3\mathrm{H}$ reaction, i.e., $N_A\langle\sigma v\rangle_{\mathrm{SBBN}} = 1.68 \times 10^8\ \mathrm{cm^3\ s^{-1}\ mole^{-1}}$ [21]. The penetration factor of the exit channel for ${}^6\mathrm{Li}(n, \alpha){}^3\mathrm{H}$ is also assumed to be $P_\alpha = 1$ because of the high Q value ($Q > E_C$). Similarly, the S factor of the ${}^4\mathrm{He}_X(t, n){}^6\mathrm{Li}_X$ reaction is derived from Eq. (16) to be

$$S_{{}^4\mathrm{He}_X + t} = 11\ \mathrm{MeV\,barn}. \quad (18)$$

For the ${}^4\mathrm{He}_X({}^3\mathrm{He}, p){}^6\mathrm{Li}_X$ reaction, we adopt the nonresonant part of the S factor from the ${}^6\mathrm{Li}(p, \alpha){}^3\mathrm{He}$ cross section, i.e., $S_{\mathrm{SBBN}} = 3.14$ MeV barn [21]. The penetration factors of the exit channel for the ${}^6\mathrm{Li}(n, \alpha){}^3\mathrm{H}$ and ${}^4\mathrm{He}_X({}^3\mathrm{He}, p){}^6\mathrm{Li}_X$ reactions are assumed to be $P_\alpha = 1$ and $P_p = 1$ because of the high Q values ($Q > E_C$). The S factor for the ${}^4\mathrm{He}_X({}^3\mathrm{He}, p){}^6\mathrm{Li}_X$ reaction is derived using Eq. (16) to be

$$S_{{}^4\mathrm{He}_X + {}^3\mathrm{He}} = 63\ \mathrm{MeV\,barn}. \quad (19)$$

5. *Transfer reactions* $p_X(n, p)n_X$ *and* $p_X(\alpha, p){}^4\mathrm{He}_X$

Since neutron radiative X capture reactions would be relatively weak, the most important reaction for neutrons to become bound to X particles is $p_X(n, p)n_X$. In this reaction, an X particle transfers from a proton to a neutron. For this reaction, we use the rate for the ${}^7\mathrm{Be}(n, p){}^7\mathrm{Li}$ reaction, which is similar to the $p_X(n, p)n_X$ in the sense that both ${}^6\mathrm{Li}$ and X are massive and strongly interacting spectator particles so that their reactions have similar dynamics.

If p_X were to survive beyond the epoch of ${}^4\mathrm{He}$ production in the SBBN, i.e., to temperatures $T_9 \lesssim 0.1$ (although this is found not to be the case in the present network calculation), then ${}^4\mathrm{He}$ could become bound to an X particle via the reaction $p_X(\alpha, p){}^4\mathrm{He}_X$. This kind of exchange reaction plays an important role in the catalyzed BBN scenario with only electromagnetically interacting X^- particles [43]. For the rates of this reaction, we use the ${}^8\mathrm{B}(\alpha, p){}^{11}\mathrm{C}$ reaction since ${}^7\mathrm{Be}$ and X are massive and

TABLE VI. β-decay rates of X nuclei.

	Q_X (MeV)						Decay rate (s^{-1})		
Reaction	X^0 case	X^- case	X^+ case	Q (MeV)	$T_{1/2}$	Ref.	X^0 case	X^- case	X^+ case
$^1n(\beta^-)^1H$	0.782	1.643	−0.069	0.782	10.19 m	[24]	1.133×10^{-3}	4.634×10^{-2}	⋯
$^3H(\beta^-)^3He$	1.825	2.608	1.044	0.019	(12.3 ± 0.1) y	[44]	1.626×10^{1}	9.700×10^{1}	9.954×10^{-1}
$^5Li(\beta^+)^5He$	0.726	0.042	1.409	−0.732	⋯	[45]	⋯	⋯	⋯
$^6He(\beta^-)^6Li$	2.127	2.815	1.439	3.508	(806.7 ± 1.5) ms	[46]	7.033×10^{-2}	2.860×10^{-1}	9.983×10^{-3}
$^6Be(\beta^+)^6Li$	3.437	2.746	4.126	3.266	⋯	[45]	7.757×10^{-1}	2.525×10^{-1}	1.934
$^7Be(\beta^+)^7Li$	0.006	−0.651	0.662	−0.160	⋯	[45]	⋯	⋯	⋯
$^8Li(\beta^-)^8Be$	15.598	16.253	14.945	16.005	(839.9 ± 0.9) ms	[47]	7.255×10^{-1}	8.912×10^{-1}	5.857×10^{-1}
$^8B(\beta^+)^8Be$	16.023	15.497	16.547	17.980	(770 ± 3) ms	[47]	5.059×10^{-1}	4.281×10^{-1}	5.943×10^{-1}
$^9B(\beta^+)^9Be$	−0.463	−0.976	0.049	0.046	⋯	[45]	⋯	⋯	⋯
$^{10}Be(\beta^-)^{10}B$	1.806	2.204	1.409	0.556	$(1.51 \pm 0.04) \times 10^6$ y	[47]	5.263×10^{-12}	1.423×10^{-11}	1.520×10^{-12}
$^{10}C(\beta^+)^{10}B$	3.564	2.612	4.512	2.626	(19.290 ± 0.012) s	[47]	1.655×10^{-1}	3.497×10^{-2}	5.381×10^{-1}
$^{11}C(\beta^+)^{11}B$	1.873	0.917	2.825	0.960	(1223.1 ± 1.2) s	[48]	1.602×10^{-2}	4.501×10^{-4}	1.250×10^{-1}
$^{12}B(\beta^-)^{12}C$	13.149	13.892	12.410	13.370	(20.20 ± 0.02) ms	[48]	3.157×10^{1}	4.155×10^{1}	2.363×10^{1}
$^{12}N(\beta^+)^{12}C$	15.293	14.768	15.814	16.316	(11.000 ± 0.016) ms	[48]	4.557×10^{1}	3.828×10^{1}	5.389×10^{1}
$^{13}N(\beta^+)^{13}C$	0.981	0.245	1.712	1.199	(9.965 ± 0.0004) m	[34]	4.250×10^{-4}	4.127×10^{-7}	6.896×10^{-3}
$^{14}C(\beta^-)^{14}N$	1.268	1.871	0.670	0.156	(5730 ± 40) y	[34]	1.340×10^{-7}	9.377×10^{-7}	5.519×10^{-9}
$^{14}O(\beta^+)^{14}N$	4.558	3.807	5.305	4.121	(70.606 ± 0.018) s	[34]	1.624×10^{-2}	6.606×10^{-3}	3.470×10^{-2}
$^{15}O(\beta^+)^{15}N$	1.609	0.857	2.355	1.732	(122.24 ± 0.16) s	[34]	3.922×10^{-3}	1.683×10^{-4}	2.638×10^{-2}

strongly interacting spectators in the reactions. Furthermore the cross section is corrected for Coulomb penetration factors using Eq. (16). The following relation is then derived:

$$S_{p_X+\alpha} = 5.1 \times 10^{-4} S_{^8\mathrm{B}+\alpha}. \quad (20)$$

Based upon the S factor for the $^8B(\alpha, p)^{11}C$ reaction ($S_{\mathrm{SBBN}} = 8.88 \times 10^4$ MeV barn), we obtain $S_{p_X+\alpha} =$ 45 MeV barn.

6. β decay of X nuclei

When Q values are larger than the electron mass in β-decay reactions, decay rates Γ scale as the fifth power of the Q values, i.e., $\Gamma \propto Q^5$. To estimate the β-decay rates for X nuclei, we use β-decay rates Γ of corresponding normal nuclei corrected for the phase-space factors, i.e.,

$$\Gamma_X = \Gamma\left(\frac{Q_X}{Q}\right)^5 = \frac{\ln 2}{T_{1/2}}\left(\frac{Q_X}{Q}\right)^5, \quad (21)$$

where $T_{1/2}$ is the half life of the normal nuclide, Q_X and Q are the Q values for the β decay of the X and normal nuclide, respectively. We show the adopted β-decay rates in Table VI. The $^6He(\beta^-)^6Li$ reaction rate is used to estimate the $^6Be_X(\beta^+)^6Li_X$ reaction. We neglect the reactions $^5Li_X(\beta^+)^5He_X$, $^7Be_X(\beta^+)^7Li_X$, $^9B_X(\beta^+)^9Be_X$, and in the X^+ case, $p_X(\beta^+)n_X$ since the Q values for these reactions are relatively small and their lifetimes would not be short compared to the BBN time scale.

When the Q value is $\lesssim 1$ MeV, atoms can decay predominantly by electron capture [39]. However, the electron capture can be neglected since we are considering only the high energy epoch of the early universe when the nuclei and X nuclei are fully ionized.

D. Reaction network

The reaction network for bound X nuclei is shown in Fig. 1. Solid arrows show nuclear reactions in the direction of positive Q value while dashed arrows indicate $\beta^\pm$ decays. The network code includes reactions up to oxygen isotopes. However, we did not find significant nuclear flow beyond the nitrogen isotopes. Hence, this network code is more than large enough to calculate the evolution of the

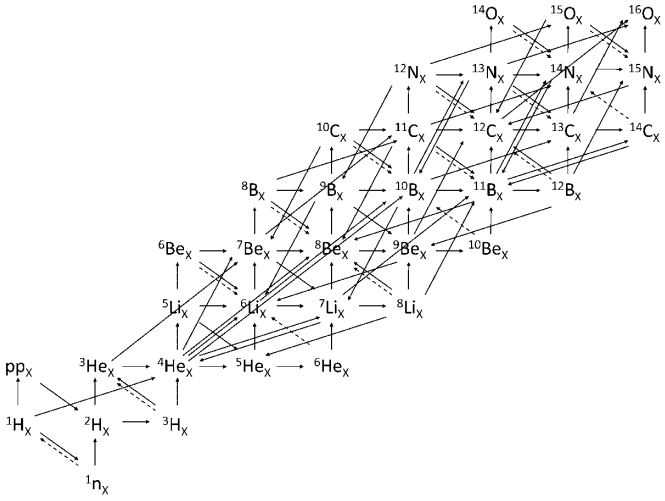

FIG. 1. Reaction pathways for the X nuclei. Solid arrows indicate the nuclear reactions, while dashed arrows indicate $\beta^\pm$ decays. Arrows are drawn in the direction of positive Q value.

nuclear abundances. The adopted nuclear reaction rates are summarized in Tables III, IV, V, and VI. In our code, radiative X-capture reactions are also included although they are not explicitly shown on Fig. 1.

III. RESULTS

A. BBN calculation result

Figures 2(a) and 2(b) show results of a BBN calculation for the case $Y_X \equiv N_X/n_b = 10^{-8}$, where N_X and n_b are the number densities of the X^0 particles and baryons, respectively. The time evolution of the abundances of normal nuclei and X nuclei are displayed in Figs. 2(a) and 2(b).

At high temperatures $100 \gtrsim T_9 \gtrsim 10$, neutrons and protons are the main constituents of baryonic matter in the universe since photonuclear reactions dissociate bound nuclei at these temperatures. However, as the temperature decreases, bound nuclei can form. At $T_9 \sim 5$ ($T \sim 0.4$ MeV, $t \sim 4$ s) X^0 particles capture nucleons so that the X^0 abundance suddenly decreases [Fig. 2(b)]. The X^0 particles first predominantly capture protons to form ${}^1\mathrm{H}_X$. This is because only protons and neutrons exist in significant amounts during that epoch. Also, neutron-capture reactions are hindered as explained in Sec. II C 1. The ${}^1\mathrm{H}_X$ nuclei then interact strongly with background neutrons through the photonless ${}^1\mathrm{H}_X(n, p)n_X$ transfer reaction so that n_X is also produced. These n_X nuclei then capture protons to form ${}^2\mathrm{H}_X$. As heavier X nuclei are transformed into other nuclei with decreased proton number through (n, p) reactions, they lead to the formation of heavier X nuclei via the reaction pathways shown in Fig. 1. High energy nuclear reactions produce abundant ${}^2\mathrm{H}_X$ and slowly increasing abundances of ${}^3\mathrm{He}_X$, ${}^4\mathrm{He}_X$, and ${}^5\mathrm{He}_X$ [Fig. 2(b)]. The production of ${}^2\mathrm{H}_X$ via the $pp_X(n, p)^2\mathrm{H}_X$ reaction is also operative. The X nuclei increase their nucleon number gradually until the temperature decreases to $T_9 \sim 1$ ($T \sim 0.1$ MeV, $t \sim 170$ s). Then at $T_9 \sim 1$, a drastic increase in the nucleosynthesis of X nuclei occurs.

Nuclear reactions at low temperature are important in determining the final elemental abundances for normal nuclides. Reactions at relatively low temperatures, however, are hindered by the Coulomb barriers. Nuclides with small atomic numbers, therefore, are more easily processed at low temperature. In addition, reactions triggered by abundant nuclides play important roles in nucleosynthesis since the reaction rates are proportional to the abundances of the reactant nuclei.

In BBN, the abundance of deuterium is very high at $T_9 \sim 1$ [Fig. 2(a)]. Reactions of X nuclei triggered by deuterons are, therefore, efficient at this epoch both because deuterium is very abundant and because its charge is low. The most important point is that strong photonless nuclear reactions to increase mass numbers exist, i.e., (d, n) and (d, p) reactions. These reactions help X nuclei to capture more nucleons and become more deeply bound. In this way, X nuclei are processed at $T_9 \sim 1$ and heavy X nuclei up to ${}^{13}\mathrm{C}_X$ are produced in individual abundances of $10^{-14} \lesssim A_X/\mathrm{H} \lesssim 10^{-8}$ [Fig. 2(b)].

This model of BBN with the strongly interacting X^0 particles changes an important aspect in SBBN which is that the nuclides ^{5}He and ^{5}Li are unstable to the particle decay so that they limit the production of heavier nuclei. However, if they are stabilized against particle emission by binding with an X^0, then (d, n) and (d, p) reactions subsequently link ${}^4\mathrm{He}_X$ with ${}^5A_X$, ${}^5A_X$ with ${}^6B_X$, and so on. Light element production is thus catalyzed by X^0 particles.

Yields of light nuclides from lithium to carbon are significant in this model. The reactions contributing to the production and destruction of light nuclides are summarized in Table VII. The last column in the table shows the resulting yields for the case of $Y_X = 10^{-8}$ and a long lifetime compared to the duration of nucleosynthesis; $\tau_X \gg 10^4$ sec. Nuclides of mass numbers up to 10 are produced in abundances larger than $A/\mathrm{H} = 10^{-11}$.

The production of nuclides with $A > 10$ is not significant through the (d, n) and (d, p) reactions. Small amounts of ${}^{12}\mathrm{C}_X$ and ${}^{13}\mathrm{C}_X$ are produced, however, via the (α, n) and (α, p) reactions. The ${}^6\mathrm{Li}_X$ production reaction in this paradigm is ${}^5\mathrm{He}_X(d, n){}^6\mathrm{Li}_X$ while that of ^{6}Li in SBBN is the ${}^4\mathrm{He}(d, \gamma){}^6$Li reaction. This latter cross section is very small due to the associated hindered transition rate through an electric quadrupole transition. The ${}^7\mathrm{Be}_X$ production reaction is ${}^6\mathrm{Li}_X(p, \gamma){}^7\mathrm{Be}_X$ while that of ^{7}Be in SBBN is ${}^4\mathrm{He}({}^3\mathrm{He}, \gamma){}^7$Be whose rate is smaller than the former reaction because of the smaller abundance of the target nuclide and the larger Coulomb barrier. The X nuclides ${}^9\mathrm{Be}_X$, ${}^{10}\mathrm{B}_X$, and ${}^{11}\mathrm{B}_X$ are produced through (d, n) and (d, p) reactions, while the nuclides ^{9}Be, ^{10}B, and ^{11}B in the present Galaxy are thought to be produced mainly through nuclear spallation processes of heavier CNO isotopes in the Galactic interstellar medium [49–51] or via the ν process in supernova to produce ^{11}B [52,53] except for nonstandard baryon-inhomogeneous BBN [54].

An interesting point regarding boron production in BBN with X^0 particles is that the production of ${}^{10}\mathrm{B}_X$ is preferred over that of ${}^{11}\mathrm{B}_X$. This would imply more abundant ^{10}B than ^{11}B after X^0 decay. There are no processes that predict preferential production of ^{10}B in standard processes to synthesize boron isotopes. Galactic cosmic ray spallation nucleosynthesis predicts a ratio of ${}^{11}\mathrm{B}/{}^{10}\mathrm{B} \sim 2.5$ (e.g., [49–51]). Supernova nucleosynthesis in massive stars produces large amounts of ^{11}B relative to ^{10}B through neutrino interactions ${}^{12}\mathrm{C}(\nu, \nu' n){}^{11}\mathrm{C}$ and ${}^{12}\mathrm{C}(\nu, \nu' p){}^{11}\mathrm{B}$ in the carbon layers and ${}^7\mathrm{Li}(\alpha, \gamma){}^{11}\mathrm{B}$ and ${}^7\mathrm{Be}(\alpha, \gamma){}^{11}\mathrm{C}$ in the helium layers [52,53].

We note some important differences between BBN with strongly interacting X^0 particles and BBN with negatively charged leptonic X^- particles that only interact electromagnetically, i.e. no strong interaction. First, the formation epoch of X nuclei in the X^0 case begins at $T_9 \sim 5$ which is much earlier than in the X^- case which begins for $T_9 \lesssim 0.5$

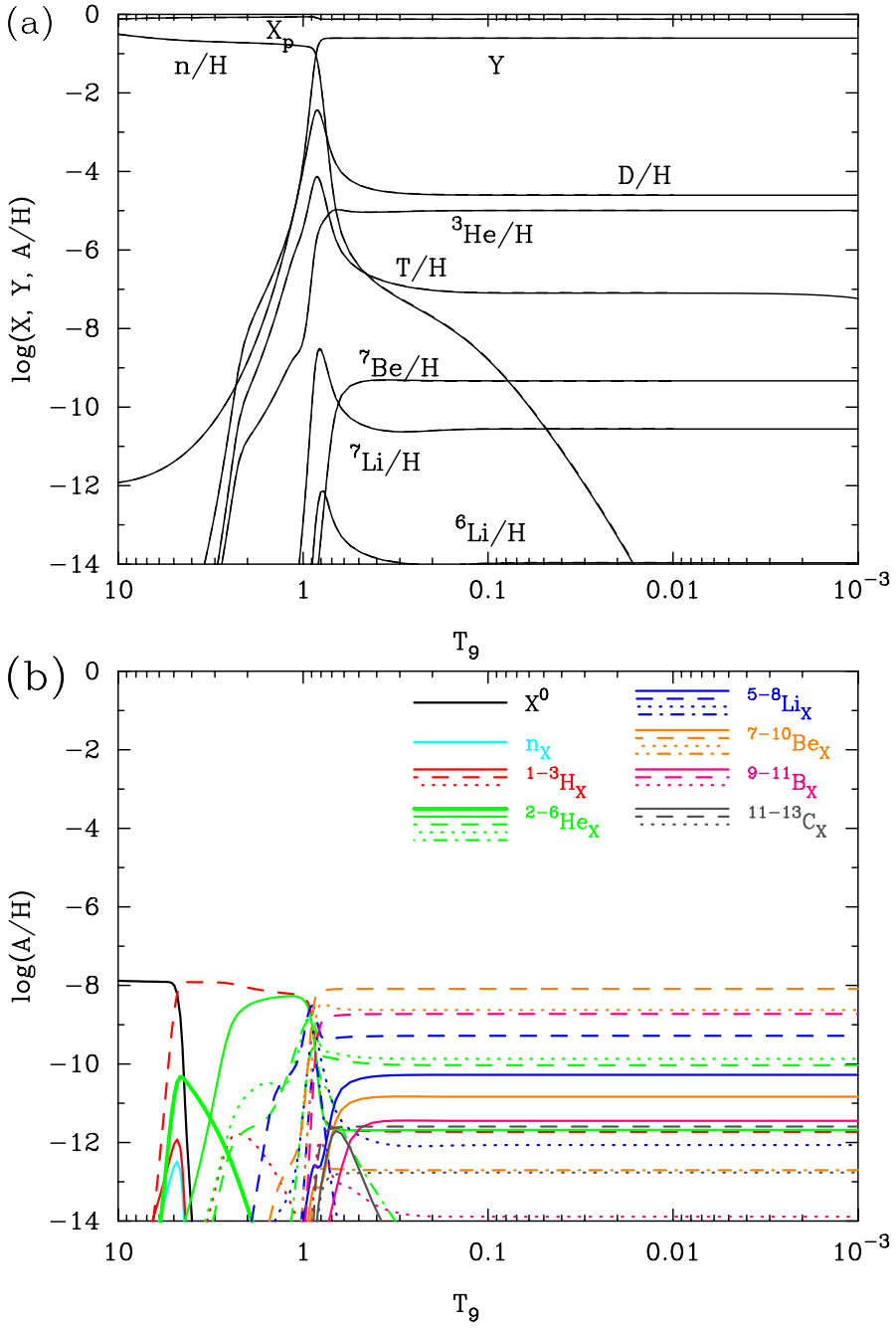

FIG. 2 (color online). Calculated abundances of normal nuclei (a) and X nuclei (b) as a function of T_9. For this figure we take the X^0 abundance to be $Y_X = N_X/n_b = 10^{-8}$, and its lifetime is taken to be long $\tau_X = \infty$. We utilize the X^0 reaction rates as described in the text. The dashed lines in the upper figure (a) correspond to the abundances of normal nuclei in the SBBN model. These are nearly indistinguishable from the solid lines.

[25]. This derives from the fact that the binding energies of nuclides and X^0 particles are of the order of $\sim$10 MeV which is much larger than the electromagnetic binding of nuclides with X^- particles ($\sim$ 1 MeV). X nuclei produced in such a high energy environment have a better chance to be processed so that many species of X nuclei are produced in considerable abundance. In the X^- case, on the other hand, the temperature of the universe is already so low that, when the X nuclei finally form, they can hardly be processed through subsequent nuclear reactions except for the special cases of the resonant ${}^7\mathrm{Be}_X(p,\gamma){}^8\mathrm{B}_X$ reaction [55] and the X^--catalyzed transfer reaction ${}^4\mathrm{He}_X(d, X^-){}^6\mathrm{Li}$ [56]. As a result, nuclides heavier than the beryllium isotopes are not produced in significant amounts in that paradigm.

This result for the time evolution of the X-nuclei abundances was not predicted precisely in the analytic estimation of previous studies [19,20]. Dicus and Teplitz [19]

TABLE VII. Most important reactions for the production and destruction of light nuclides.

Nuclide	Production	Destruction	Yield A/H
^6Li_X	$^5He_X(d, n)^6Li_X$	$^6Li_X(d, p)^7Li_X$	5×10^{-10}
^7Be_X	$^6Li_X(p, \gamma)^7Be_X$	$^7Be_X(n, p)^7Li_X$	1×10^{-11}
^8Be_X	$^8Li_X(p, n)^8Be_X$	$^8Be_X(d, p)^9Be_X$	8×10^{-9}
^9Be_X	$^8Be_X(d, p)^9Be_X$	$^9Be_X(d, n)^{10}B_X$	2×10^{-9}
$^{10}B_X$	$^9Be_X(d, n)^{10}B_X$	$^{10}B_X(d, n)^{11}C_X$	2×10^{-9}
$^{11}B_X$	$^{10}B_X(d, p)^{11}B_X$	$^{11}B_X(p, \alpha)^8Be_X$	1×10^{-14}
$^{12}C_X$	$^9Be_X(\alpha, n)^{12}C_X$	...	3×10^{-12}
$^{13}C_X$	$^{10}B_X(\alpha, p)^{13}C_X$	...	2×10^{-13}

deduced that the stable hadrons would be preferentially locked into beryllium. Our result, however, shows that many light elements including beryllium are produced abundantly and beryllium is not particularly more abundant than other nuclides. In the study of [19], the strong photonless reactions (d, n) and (d, p) were not included. This is the reason for the large difference between that work and our present results for BBN.

In the present work we have shown that most of the X^0 particles end up in X nuclei after BBN in contrast to the estimation in [20]. We note, however, that the X capture reaction rates adopted in the present study are only approximate and should be calculated more precisely in a more thorough quantum mechanical treatment in the future. We have shown that strongly interacting X^0 particles undergo efficient X capture by protons at $T_9 \sim 5$. This leads to the subsequent production of ^2H_X, ^3He_X, ^4He_X, and so on. This does not occur through normal nuclei like ^2H, ^3He, and ^4He, but through X nuclei from ^1H_X. This reaction flow was not considered in [20]. Although our result includes some uncertainty in the binding energies and nuclear reaction rates of X nuclei (originating from our assumption of the interaction strength), we nevertheless expect that the X^0 particles will end up in X nuclei after BBN as long as the interaction strength is very large compared to electromagnetic strength.

The calculated BBN abundances of light nuclides depend strongly on the X^0 abundance, Y_X. As an example, a series of BBN calculations was carried out varying Y_X as a parameter with no change in the assumption of large τ_X. Although the decay lifetime of X^0 is assumed to be much longer than the time scale of BBN $\gtrsim 10^4$ s, the X^0 particles are assumed to have been long extinct by now. The final abundances of stable nuclides are obtained by removing the X^0 from the X nuclei, A_X, and allowing A to decay to a stable nucleus. The interaction of the decay products with the remaining A spectator nucleus and the nonthermal nucleosynthesis triggered by high energy decay products are neglected here. Such effects, however, should be studied in the future.

Figure 3 shows the calculated abundance ratios of $^6Li/H$ and $^7Li/H$ (solid curves) as a function of Y_X. The dashed lines correspond to the mean values measured in MPHSs,

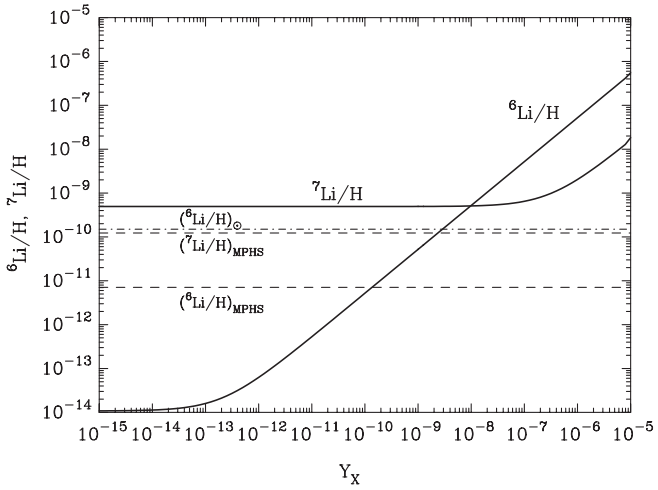

FIG. 3. Calculated abundances of $^6Li/H$ and $^7Li/H$ as a function of the X^0 abundance Y_X. The dashed lines indicate the mean values observed in MPHSs.

i.e., $^6Li/H = (7.1 \pm 0.7) \times 10^{-12}$ [57] and $^7Li/H = 1.23^{+0.68}_{-0.32} \times 10^{-10}$ [58], respectively. The ^6Li and ^7Li abundances both increase linearly with Y_X. However, the final ^6Li_X and ^7Li_X abundances per X particle are independent of Y_X. As is shown in Fig. 2, the additional ^6Li is produced mainly from ^6Li_X while the additional ^7Li is from ^7Be_X. Comparing this with the case of BBN with a negatively charged leptonic X^- particle [25], we find that both cases prefer the production of ^6Li to that of ^7Li. The difference between the two cases is the relative efficiency of X-catalyzed nucleosynthesis. The efficiency of ^6Li production in the X^0 case is $\sim 10^4$ times larger than in the X^- case when the abundance of the X particle (i.e. Y_X) is taken to be the same.

In order to check if there is a possibility to solve the ^6Li and ^7Li problems in the present X^0-catalyzed BBN model, a parameter search was performed over the decay lifetime τ_X and the abundance Y_X of the X^0 particle. As described below, constraints on the (τ_X, Y_X) parameter space were derived from observational limits on the primordial light element abundances. We could not find a parameter region which simultaneously resolves the two lithium problems.

B. Constraints on primordial light element abundances

Deuterium is measured in the absorption spectra of narrow line Lyman-α absorption systems in the foreground of high redshift quasistellar objects (QSOs). An analysis of well resolved DI Lyman series transitions in the spectrum of the QSO Q0931 + 072 was performed recently [59]. With the newly deduced value of the deuterium abundance, they obtained a mean value for the primordial deuterium abundance of $\log(D/H) = -4.55 \pm 0.03$. We adopt this value and a two sigma uncertainty, i.e.,

$$2.45 \times 10^{-5} < D/H < 3.24 \times 10^{-5}. \quad (22)$$

^{3}He is measured in Galactic HII regions by the 8.665 GHz hyperfine transition of $^3He^+$ [60]. A plateau with a relatively large dispersion with respect to metallicity has been found at a level of $^3\mathrm{He/H} = (1.9 \pm 0.6) \times 10^{-5}$. However, it is not yet understood whether ^{3}He has increased or decreased through the course of stellar and galactic evolution [61,62]. Nevertheless, it does not seem that the cosmic averaged ^{3}He abundance has decreased from that produced in BBN by more than a factor of 2 due to burning in stars. Because both the observations and theoretical predictions of the primordial deuterium abundance are consistent with each other, the deuteron abundance appears not to have decreased since the epoch of BBN. ^{3}He is more resistant to the stellar burning. Therefore, its abundance would not have decreased significantly. Thus, we adopt a two sigma upper limit from Galactic HII region abundances of

$$^3\mathrm{He/H} < 3.1 \times 10^{-5}. \quad (23)$$

We do not give a lower limit due to the large uncertainty in the Galactic production of ^{3}He.

For the primordial helium abundance we adopt $Y = 0.2477 \pm 0.0029$ from an analysis [63] of the primordial mass fraction based upon new atomic physics computations of the recombination coefficients for HeI and of the collisional excitations of the HI Balmer lines, together with observations and photoionization models of metal-poor extragalactic HII regions. We adopt the following range for the primordial ^{4}He abundance within the conservative two sigma limits of

$$0.2419 < Y < 0.2535. \quad (24)$$

An upper limit on the ^{6}Li abundance is taken which allows for the possible depletion on stellar surfaces of up to a factor of $\sim$10 above the observed plateau abundance of $^6\mathrm{Li/H} = (7.1 \pm 0.7) \times 10^{-12}$ [57]. This upper limit is not larger than the solar abundance of $^6\mathrm{Li/H}_\odot = 1.7 \times 10^{-10}$ [64] which represents a typical present abundance. We do not take the lower limit on the observations as a lower limit for the production of ^{6}Li by X particles, because of the current controversy as to whether the ^{6}Li observation is actually a primordial abundance. Hence, the lower limit of ^{6}Li for our purposes is zero. The adopted constraint on the ^{6}Li abundance is thus

$$^6\mathrm{Li/H} < 10^{-10}. \quad (25)$$

An upper limit on the ^{7}Li abundance is taken to be 6.15×10^{-10} considering a possible depletion of up to a factor of $\sim$5 down to the observationally determined value of $^7\mathrm{Li/H} = (1.23^{+0.68}_{-0.32}) \times 10^{-10}$ [58]. A lower limit is taken from the two sigma uncertainty in the same observed value. The adopted constraint on the ^{7}Li abundance is therefore

$$0.59 \times 10^{-10} < {}^7\mathrm{Li/H} < 6.15 \times 10^{-10}. \quad (26)$$

We adopt minimum abundances observed in MPHSs as constraints on abundances of ^{9}Be, B, and C, i.e.,

$$^9\mathrm{Be/H} < 10^{-13}, \quad (27)$$

from [65–69],

$$\mathrm{B/H} < 10^{-12}, \quad (28)$$

from [70,71] and

$$\mathrm{C/H} < 10^{-8}, \quad (29)$$

from a compilation of observational data by Suda *et al.* [72].

C. Observational constraints on the long-lived strongly interacting particles

In order to study the effects of X^0 decay we calculated a series of BBN models in which we varied the decay life τ_X and abundance Y_X of the X^0 particle while the baryon-to-photon ratio remained fixed at $\eta = 6.3 \times 10^{-10}$ [73].

Figure 4 shows a contour of the ^{4}He mass fraction $Y = 0.2419$ (red line) in the (τ_X, Y_X) plane. Above this contour, $Y < 0.2419$ which breaks our adopted limit on the primordial ^{4}He abundance. Also shown are the contours for the upper limits of $\mathrm{D/H} \leq 3.24 \times 10^{-5}$ (black line), $^3\mathrm{He/H} \leq 3.1 \times 10^{-5}$ (green line), $^6\mathrm{Li/H} \leq 10^{-10}$ (blue solid line), $^7\mathrm{Li/H} \leq 6.15 \times 10^{-10}$ (purple line), $^9\mathrm{Be/H} \leq 10^{-13}$ (pink line), $\mathrm{B/H} \leq 10^{-12}$ (orange line), and $\mathrm{C/H} \leq 10^{-8}$ (gray line). The contours for the lower limit of $\mathrm{D/H} \geq 2.45 \times 10^{-5}$ are drawn by other black lines. The blue dashed lines correspond to the observed level of the ^{6}Li

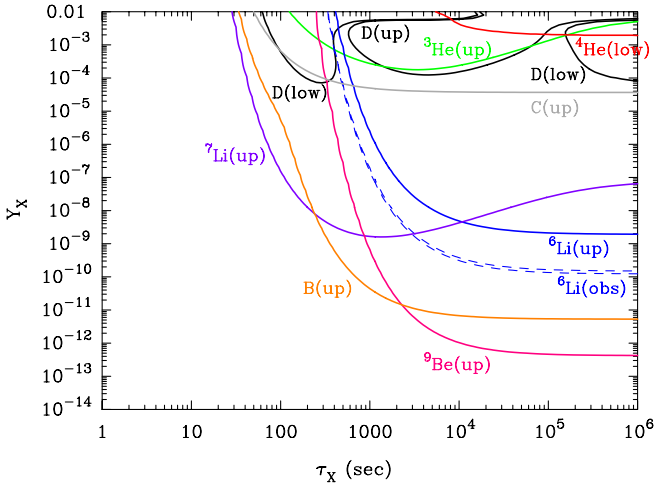

FIG. 4 (color online). Contours in the (τ_X, Y_X) plane corresponding to the adopted constraints for the primordial abundances. Contours for the mass fraction of ^{4}He, $Y = 0.2419$ (red line) and the number ratios of $^3\mathrm{He/H} = 3.1 \times 10^{-5}$ (green line), $\mathrm{D/H} = 3.24 \times 10^{-5}$ and $\mathrm{D/H} = 2.45 \times 10^{-5}$ (black lines), $^6\mathrm{Li/H} \approx 10^{-10}$ (blue solid line) and $^6\mathrm{Li/H} = (7.1 \pm 0.7) \times 10^{-12}$ (blue dashed lines), $^7\mathrm{Li/H} = 6.15 \times 10^{-10}$ (purple line), $^9\mathrm{Be/H} = 10^{-13}$ (pink line), $\mathrm{B/H} = 10^{-12}$ (orange line), and $\mathrm{C/H} = 10^{-8}$ (gray line) are shown.

abundance in MPHSs, i.e., $^6\mathrm{Li/H} = (7.1 \pm 0.7) \times 10^{-12}$. The upper right region surrounded by the contours is excluded based upon the observational constraints.

These constraints in the (τ_X, Y_X) parameter space can be summarized as follows. When the decay lifetime of the X^0 is short ($\tau_X < 30$ s), no constraint is imposed from the observed elemental abundances. When the decay lifetime is longer (30 s $< \tau_X <$ 200–300 s), the constraint from the upper limit on the ^{7}Li abundance is the strongest and it implies $Y_X < 10^{-8}$–10^{-2}. When the decay lifetime is longer (200–300 s $< \tau_X < 2 \times 10^3$ s), the constraint from the upper limit on the B abundance is the strongest and it implies $Y_X < 10^{-8}$–10^{-11}. Finally, when the decay lifetime is very long but still much shorter than the age of the present universe (2×10^3 s $< \tau_X \ll 4 \times 10^{17}$ s), the upper limit on the ^{9}Be abundance is the strongest constraint and it implies $Y_X < 10^{-11}$–$10^{-12.6}$. Since the relic abundance of the strongly interacting X particles is estimated to be $Y_X \sim 10^{-8}$ [Eq. (1)], the decay lifetime should be $\tau_X \lesssim 200$ s. Thus, models suggesting long-lived colored particles with $\tau_X \gtrsim 200$ s are rejected.

The shapes of the contours on Fig. 4 reflect the formation epochs for the X nuclides (see Fig. 2). We are not interested in the case of a large abundance of Y_X. This is because the relic abundance of a long-lived SIMP cannot be very large [see Eq. (1)] although there are significant influences of X^0 particles on light element abundances if the lifetime τ_X is long. In the lifetime region of 30 s $< \tau_X <$ 200–300 s, $^7\mathrm{Li}_X$ overproduction is the cause of the exclusion through the ^{7}Li abundance constraint. One can see that the abundance of $^7\mathrm{Li}_X$ has a peak at $T_9 \sim 1$ and is destroyed below this temperature (Fig. 2). $^{10}\mathrm{B}_X$ and $^9\mathrm{Be}_X$ form at $T_9 \lesssim 1$ in almost the same amounts. In the longest lifetime case ($2 \times 10^3 s < \tau_X \ll 4 \times 10^{17} s$) the constraint from ^{9}Be is stronger than that from B, since the observed minimum abundance of ^{9}Be is about 1 order of magnitude lower than that of B.

A new solution to the ^{6}Li or ^{7}Li problems was not found in this work. In the reactions included in our BBN calculation, there are no reactions which can effectively destroy ^{7}Li or ^{7}Be. When a large amount of ^{6}Li is produced in this X^0 catalyzed BBN, the abundances of coproduced beryllium and boron are unrealistically high, and are therefore excluded. The $^6\mathrm{Li}_X$ abundance has a peak at $T_9 \sim 1$ in Fig. 2(b). Even if the X^0 particles decay during this epoch, the remaining ^{6}Li is easily destroyed via the $^6\mathrm{Li}(p, \alpha)^3\mathrm{He}$ reaction which also destroys the ^{6}Li produced via the $^4\mathrm{He}(d, \gamma)^6\mathrm{Li}$ reactions in the SBBN. Hence, the preferential production of ^{6}Li is impossible in this model, although corrections for effects of X^0 decay may resolve this as found in Refs. [3,8,9].

IV. CONCLUSIONS

We have investigated the effects on BBN of a hypothetical long-lived strongly interacting massive particle (SIMP) X^0. The strength of the interaction between the X^0 particle and normal nuclei is assumed to be similar to that between normal nuclei. Under this assumption, binding energies of X particles to nuclei have been estimated from the Schrödinger equation with a nuclear and Coulomb potential. Using these binding energies, the reaction Q values for many nuclear reactions involving nuclei bound to X (X nuclei) were calculated. Reaction rates for X capture by nuclei, and the nuclear reaction rates of X nuclei were estimated using information from existing reaction rates of normal nuclei. We calculated the light element nucleosynthesis simultaneously taking into account X capture by nuclides and the nuclear reactions of X nuclei along with the standard nuclear reactions. The conclusions are as follows.

First, some X nuclides like $^5\mathrm{He}_X$, $^5\mathrm{Li}_X$, and $^8\mathrm{Be}_X$ are stabilized against particle decay since the binding energies of nuclei and X particles are very large $\sim O$ (10 MeV) and the total binding energies of X nuclei (i.e. the binding energies of nuclei from separate nucleons plus the binding energies of X nuclei from separate X particles and nuclei) change significantly from those of normal nuclei. Accordingly, there are several reactions whose Q values become negative when nuclides are bound to X particles.

Second, at $T_9 \sim 5$, the X^0 particles capture nucleons so that the free X^0 abundance decreases suddenly. Then high energy nuclear reactions produce abundant $^2\mathrm{H}_X$. The X nuclei then increase their nucleon number gradually until the temperature decreases to $T_9 \sim 1$. When the abundance of deuterium becomes high at $T_9 \sim 1$, strong photonless nuclear reactions [i.e. (d, n) and (d, p)] produce heavier X nuclei up to $^{13}\mathrm{C}_X$.

Third, from a comparison between BBN with X^0 particles and BBN with negatively charged leptonic X^- particles, we find that the bound state of X nuclei forms earlier in the X^0 case ($T_9 \sim 5$) than in the X^- case ($T_9 \lesssim 0.5$). This is due to the larger binding energies of nuclei and X^0 particles. Since X nuclei are produced in a high energy environment, they can be processed to heavier X nuclei which are produced in considerable amounts.

Fourth, we do not find a solution to the ^{6}Li or ^{7}Li problem in this BBN model with the X^0 particles. There is a possibility that ^{6}Li is produced in an abundance even more than that observed in MPHSs. However, the coproduced abundances of heavier beryllium and boron nuclides constrain this possibility.

Fifth, constraints on the lifetime and abundance of the X^0 particle are derived. The following constraints on the abundance [$Y_X < 10^{-8}$–10^{-2} (for 30 s $< \tau_X <$ 200–300 s), $Y_X < 10^{-8}$–10^{-11} (for 200–300 s $< \tau_X < 2 \times 10^3$ s), and $Y_X < 10^{-11}$–$10^{-12.6}$ (for 2×10^3 s $< \tau_X \ll 4 \times 10^{17}$ s)] have been deduced based upon the observational constraints on primordial light element abundances. These constraints reject models with long-lived ($\tau_X \gtrsim 200$ s) colored particles based upon their relic abundance, i.e., $Y_X \sim 10^{-8}$.

Although we made an assumption about the interaction strength of the X^0 particle, the magnitude of the effect of long-lived SIMPs on BBN would not change by more than a few orders of magnitude from the result of this study unless the interaction strength is much smaller. We also expect that the result would not change by many orders even if a SIMP has a charge of $\pm e$. This is because the nucleosynthesis of X nuclei occurs very early in the universe when the nuclear reactions are not significantly hindered by the Coulomb barriers. More realistic estimates of the reaction rates utilizing a quantum mechanical treatment would be necessary to more precisely study the effect of X^0 particles on BBN. Moreover, the direct interactions of decay products with the remaining nuclei A in the decay of X^0 in an X nucleus A_X should be studied in the future in order to better estimate final abundances of the light elements after the X^0 decay. Nevertheless, the calculated light element abundances in this study should not change by more than an order of magnitude from the effects of the decay of X^0 considering the fact that the cross section for the elastic scattering of pions by ^{12}C is roughly one-half of the total cross section so that half of the ^{12}C nuclei are left intact even when effects of the hadronic decay are included [74].

ACKNOWLEDGMENTS

We are very grateful to Professor Masayasu Kamimura for helpful discussions and suggestions regarding the nuclear reactions. We would like to thank Professor Richard N. Boyd for careful reading of the manuscript and valuable comments. This work has been supported in part by the Mitsubishi Foundation, the Grant-in-Aid for Scientific Research under Contracts No. 20105004 and No. 20244035 of the Ministry of Education, Science, Sports and Culture of Japan, and the JSPS Core-to-Core Program, International Research Network for Exotic Femto Systems (EFES). M. K. acknowledges the support by JSPS Grant-in-Aid under Contract No. 18.11384. Work at the University of Notre Dame was supported by the U.S. Department of Energy under Nuclear Theory Grant No. DE-FG02-95-ER40934.

[1] J. Ellis, D. V. Nanopoulos, and S. Sarkar, Nucl. Phys. **B259**, 175 (1985); R. H. Cyburt, J. Ellis, B. D. Fields, and K. A. Olive, Phys. Rev. D **67**, 103521 (2003); J. R. Ellis, K. A. Olive, and E. Vangioni, Phys. Lett. B **619**, 30 (2005).

[2] N. Terasawa, M. Kawasaki, and K. Sato, Nucl. Phys. **B302**, 697 (1988); M. Kawasaki, P. Kernan, H.-S. Kang, R. J. Scherrer, G. Steigman, and T. P. Walker, Nucl. Phys. **B419**, 105 (1994); M. Kawasaki and T. Moroi, Prog. Theor. Phys. **93**, 879 (1995); E. Holtmann, M. Kawasaki, and T. Moroi, Phys. Rev. Lett. **77**, 3712 (1996); M. Kawasaki, K. Kohri, and T. Moroi, Phys. Rev. D **63**, 103502 (2001); M. Kawasaki, K. Kohri, and T. Moroi, Phys. Lett. B **625**, 7 (2005); Phys. Rev. D **71**, 083502 (2005); T. Kanzaki, M. Kawasaki, K. Kohri, and T. Moroi, Phys. Rev. D **75**, 025011 (2007); M. Kawasaki, K. Kohri, T. Moroi, and A. Yotsuyanagi, Phys. Rev. D **78**, 065011 (2008).

[3] D. Cumberbatch, K. Ichikawa, M. Kawasaki, K. Kohri, J. Silk, and G. D. Starkman, Phys. Rev. D **76**, 123005 (2007); K. Kohri and Y. Santoso, Phys. Rev. D **79**, 043514 (2009).

[4] M. H. Reno and D. Seckel, Phys. Rev. D **37**, 3441 (1988).

[5] S. Dimopoulos, R. Esmailzadeh, G. D. Starkman, and L. J. Hall, Phys. Rev. Lett. **60**, 7 (1988); S. Dimopoulos, R. Esmailzadeh, L. J. Hall, and G. D. Starkman, Astrophys. J. **330**, 545 (1988); Nucl. Phys. **B311**, 699 (1989).

[6] M. Y. Khlopov, Y. L. Levitan, E. V. Sedelnikov, and I. M. Sobol, Phys. At. Nucl. **57**, 1393 (1994); E. V. Sedelnikov, S. S. Filippov, and M. Y. Khlopov, Phys. At. Nucl. **58**, 235 (1995).

[7] K. Jedamzik, Phys. Rev. Lett. **84**, 3248 (2000); Phys. Rev. D **70**, 083510 (2004); K. Jedamzik, K. Y. Choi, L. Roszkowski, and R. Ruiz de Austri, J. Cosmol. Astropart. Phys. 07 (2006) 007; K. Jedamzik, Phys. Rev. D **74**, 103509 (2006).

[8] K. Jedamzik, Phys. Rev. D **70**, 063524 (2004).

[9] M. Kusakabe, T. Kajino, and G. J. Mathews, Phys. Rev. D **74**, 023526 (2006); M. Kusakabe, T. Kajino, T. Yoshida, T. Shima, Y. Nagai, and T. Kii, Phys. Rev. D **79**, 123513 (2009).

[10] N. Arkani-Hamed and S. Dimopoulos, J. High Energy Phys. 06 (2005) 073.

[11] N. Arkani-Hamed, S. Dimopoulos, G. F. Giudice, and A. Romanino, Nucl. Phys. **B709**, 3 (2005).

[12] S. Raby, Phys. Lett. B **422**, 158 (1998).

[13] U. Sarid and S. D. Thomas, Phys. Rev. Lett. **85**, 1178 (2000).

[14] J. Kang, M. A. Luty, and S. Nasri, J. High Energy Phys. 09 (2008) 086.

[15] E. W. Kolb and M. S. Turner, *The Early Universe* (Addison-Wesley, Redwood City, CA, 1990).

[16] S. Wolfram, Phys. Lett. **82B**, 65 (1979).

[17] C. B. Dover, T. K. Gaisser, and G. Steigman, Phys. Rev. Lett. **42**, 1117 (1979).

[18] G. D. Starkman, A. Gould, R. Esmailzadeh, and S. Dimopoulos, Phys. Rev. D **41**, 3594 (1990).

[19] D. A. Dicus and V. L. Teplitz, Phys. Rev. Lett. **44**, 218 (1980).

[20] R. N. Mohapatra and V. L. Teplitz, Phys. Rev. Lett. **81**, 3079 (1998).

[21] L. H. Kawano, Report No. FERMILAB-Pub-92/04-A, 1992.

[22] M. S. Smith, L. H. Kawano, and R. A. Malaney, Astrophys. J. Suppl. Ser. **85**, 219 (1993).

[23] P. Descouvemont, A. Adahchour, C. Angulo, A. Coc, and E. Vangioni-Flam, At. Data Nucl. Data Tables **88**, 203 (2004).

[24] G. J. Mathews, T. Kajino, and T. Shima, Phys. Rev. D **71**, 021302(R) (2005).

[25] M. Kusakabe, T. Kajino, R. N. Boyd, T. Yoshida, and G. J. Mathews, Astrophys. J. **680**, 846 (2008).

[26] E. Hiyama, Y. Kino, and M. Kamimura, Prog. Part. Nucl. Phys. **51**, 223 (2003).

[27] W. M. Yao *et al.*, J. Phys. G **33**, 1 (2006).

[28] J. Martorell, D. W. L. Sprung, and D. C. Zheng, Phys. Rev. C **51**, 1127 (1995).

[29] G. G. Simon, C. Schmitt, and V. H. Walther, Nucl. Phys. **A364**, 285 (1981).

[30] A. Amroun *et al.*, Nucl. Phys. **A579**, 596 (1994).

[31] I. Tanihata *et al.*, Phys. Lett. B **206**, 592 (1988).

[32] M. Fukuda *et al.*, Nucl. Phys. **A656**, 209 (1999).

[33] A. Ozawa, T. Suzuki, and I. Tanihata, Nucl. Phys. **A693**, 32 (2001).

[34] F. Ajzenberg-Selove, Nucl. Phys. **A523**, 1 (1991).

[35] D. R. Tilley, H. R. Weller, and C. M. Cheves, Nucl. Phys. **A564**, 1 (1993).

[36] W. A. Fowler, G. R. Caughlan, and B. A. Zimmerman, Annu. Rev. Astron. Astrophys. **5**, 525 (1967).

[37] C. A. Bertulani, Comput. Phys. Commun. **156**, 123 (2003).

[38] K. Shibata *et al.*, J. Nucl. Sci. Technol. **39**, 1125 (2002).

[39] R. N. Boyd, *An Introduction to Nuclear Astrophysics* (University of Chicago Press, Chicago, IL, 2008).

[40] G. R. Caughlan and W. A. Fowler, At. Data Nucl. Data Tables **40**, 283 (1988).

[41] C. Angulo *et al.*, Nucl. Phys. **A656**, 3 (1999).

[42] D. D. Clayton, *Principles of Stellar Evolution and Nucleosynthesis* (University of Chicago Press, Chicago, IL, 1983).

[43] M. Kamimura, Y. Kino, and E. Hiyama, Prog. Theor. Phys. **121**, 1059 (2009).

[44] D. R. Tilley, H. R. Weller, and H. H. Hasan, Nucl. Phys. **A474**, 1 (1987).

[45] G. Audi, A. H. Wapstra, and C. Thibault, Nucl. Phys. **A729**, 337 (2003).

[46] D. R. Tilley *et al.*, Nucl. Phys. **A708**, 3 (2002).

[47] D. R. Tilley *et al.*, Nucl. Phys. **A745**, 155 (2004).

[48] F. Ajzenberg-Selove, Nucl. Phys. **A506**, 1 (1990).

[49] N. Prantzos, M. Casse, and E. Vangioni-Flam, Astrophys. J. **403**, 630 (1993).

[50] R. Ramaty, B. Kozlovsky, R. E. Lingenfelter, and H. Reeves, Astrophys. J. **488**, 730 (1997).

[51] M. Kusakabe, Astrophys. J. **681**, 18 (2008).

[52] S. E. Woosley and T. A. Weaver, Astrophys. J. Suppl. Ser. **101**, 181 (1995).

[53] T. Yoshida, T. Kajino, and D. H. Hartmann, Phys. Rev. Lett. **94**, 231101 (2005).

[54] T. Kajino and R. N. Boyd, Astrophys. J. **359**, 267 (1990).

[55] C. Bird, K. Koopmans, and M. Pospelov, Phys. Rev. D **78**, 083010 (2008).

[56] M. Pospelov, Phys. Rev. Lett. **98**, 231301 (2007).

[57] M. Asplund, D. L. Lambert, P. E. Nissen, F. Primas, and V. V. Smith, Astrophys. J. **644**, 229 (2006).

[58] S. G. Ryan, T. C. Beers, K. A. Olive, B. D. Fields, and J. E. Norris, Astrophys. J. **530**, L57 (2000).

[59] M. Pettini, B. J. Zych, M. T. Murphy, A. Lewis, and C. C. Steidel, Mon. Not. R. Astron. Soc. **391**, 1499 (2008).

[60] T. M. Bania, R. T. Rood, and D. S. Balser, Nature (London) **415**, 54 (2002).

[61] C. Chiappini, A. Renda, and F. Matteucci, Astron. Astrophys. **395**, 789 (2002).

[62] E. Vangioni-Flam, K. A. Olive, B. D. Fields, and M. Casse, Astrophys. J. **585**, 611 (2003).

[63] M. Peimbert, V. Luridiana, and A. Peimbert, Astrophys. J. **666**, 636 (2007).

[64] K. Lodders, Astrophys. J. **591**, 1220 (2003).

[65] A. M. Boesgaard, C. P. Deliyannis, J. R. King, S. G. Ryan, S. S. Vogt, and T. C. Beers, Astron. J. **117**, 1549 (1999).

[66] F. Primas, M. Asplund, P. E. Nissen, and V. Hill, Astron. Astrophys. **364**, L42 (2000).

[67] F. Primas, P. Molaro, P. Bonifacio, and V. Hill, Astron. Astrophys. **362**, 666 (2000).

[68] H. Ito, W. Aoki, S. Honda, and T. C. Beers, Astrophys. J. **698**, L37 (2009).

[69] A very low upper limit on the carbon-enhanced metal-poor star BD + 44°493 has been reported recently that is $^9\mathrm{Be/H} < 10^{-14}$ [68]. Our adopted constraint is therefore relatively conservative. The stronger constraint, i.e., $^9\mathrm{Be/H} < 10^{-4}$, leads to a more limited allowed parameter region of the X^0 particles.

[70] D. K. Duncan, F. Primas, L. M. Rebull, A. M. Boesgaard, C. P. Deliyannis, L. M. Hobbs, J. R. King, and S. G. Ryan, Astrophys. J. **488**, 338 (1997).

[71] R. J. Garcia Lopez, D. L. Lambert, B. Edvardsson, B. Gustafsson, D. Kiselman, and R. Rebolo, Astrophys. J. **500**, 241 (1998).

[72] T. Suda *et al.*, Publ. Astron. Soc. Jpn. **60**, 1159 (2008).

[73] J. Dunkley *et al.* (WMAP Collaboration), Astrophys. J. Suppl. Ser. **180**, 306 (2009).

[74] S. P. Rosen, Phys. Rev. Lett. **34**, 774 (1975).